

# Wearable and Stretchable Strain Sensors: Materials, Sensing Mechanisms, and Applications

Hamid Souri,\* Hritwick Banerjee, Ardian Jusufi, Norbert Radacsi, Adam A. Stokes, Inkyu Park, Metin Sitti, and Morteza Amjadi\*

Recent advances in the design and implementation of wearable resistive, capacitive, and optical strain sensors are summarized herein. Wearable and stretchable strain sensors have received extensive research interest due to their applications in personalized healthcare, human motion detection, human-machine interfaces, soft robotics, and beyond. The disconnection of overlapped nanomaterials, reversible opening/closing of microcracks in sensing films, and alteration of the tunneling resistance have been successfully adopted to develop high-performance resistive-type sensors. On the other hand, the sensing behavior of capacitive-type and optical strain sensors is largely governed by their geometrical changes under stretching/releasing cycles. The sensor design parameters, including stretchability, sensitivity, linearity, hysteresis, and dynamic durability, are comprehensively discussed. Finally, the promising applications of wearable strain sensors are highlighted in detail. Although considerable progress has been made so far, wearable strain sensors are still in their prototype stage, and several challenges in the manufacturing of integrated and multifunctional strain sensors should be yet tackled.

to soft and robust strain sensors. Wearable and stretchable strain sensors have drawn tremendous attention due to their facile interaction with the human body for a variety of applications such as health-care monitoring<sup>[2–7]</sup> and human motion detection.<sup>[8–11]</sup> Recently, soft strain sensors have shown potentials in soft robotics as sensory skins, enabling robots to actively interact with the surrounding environment, including humans.<sup>[12–14]</sup> As in the case of wearable applications, strain sensors must possess high stretchability (>50%), high sensitivity, and high durability to accommodate multiscale and dynamic deformations induced by human activities. In addition, they should be mechanically compliant to intimately conform to the curved and soft surfaces like the human skin, chemically resistant to sweating, and intact to atmospheric conditions such as variations in temperature and humidity.

To date, many stretchable strain sensors have been developed by the incorporation of advanced functional nanomaterials into stretchable supporting materials. Nanomaterials in the form of electrically conductive networks serve as active sensing films and stretchable electrodes for resistive- and capacitive-type strain sensors, respectively.<sup>[6,8,9,15–18]</sup>


## 1. Introduction

Strain sensors transduce external mechanical stimuli into electrical signals.<sup>[1]</sup> Advances in materials science and micro-/nanotechnology have translated commercial brittle strain gauges

Dr. H. Souri  
Aroa Biosurgery Limited  
Auckland 2022, New Zealand  
E-mail: hamid.souri@aroabio.com, souri6889@gmail.com

H. Banerjee, Dr. A. Jusufi  
Locomotion in Biorobotic and Somatic Systems Group  
Max-Planck Institute for Intelligent Systems  
Stuttgart 70569, Germany

Dr. N. Radacsi  
School of Engineering  
Institute for Materials and Processes  
The University of Edinburgh  
Robert Stevenson Road, Edinburgh EH9 3FB, UK

 The ORCID identification number(s) for the author(s) of this article can be found under <https://doi.org/10.1002/aisy.202000039>.

© 2020 The Authors. Published by WILEY-VCH Verlag GmbH & Co. KGaA, Weinheim. This is an open access article under the terms of the Creative Commons Attribution License, which permits use, distribution and reproduction in any medium, provided the original work is properly cited.

DOI: 10.1002/aisy.202000039

Dr. A. A. Stokes  
School of Engineering  
Institute for Integrated Micro and Nano Systems  
SMC  
EH9 3FF Edinburgh, UK

Prof. I. Park  
Department of Mechanical Engineering  
Korea Advanced Institute of Science & Technology (KAIST)  
291 Daehak-ro, Yuseong-gu, Daejeon 34141, South Korea

Prof. M. Sitti  
Physical Intelligence Department  
Max-Planck Institute for Intelligent Systems  
Stuttgart 70569, Germany

Prof. M. Amjadi  
Institute of Mechanical, Process and Energy Engineering  
Heriot-Watt University  
Edinburgh EH14 4AS, UK  
E-mail: m.amjadi@hw.ac.uk

In stretchable optical sensors, nanomaterials with unique optical properties are utilized to enhance the optical sensitivity of sensors.<sup>[1,19,20]</sup> On the other hand, elastomers and textiles are typically used as supporting substrates given their high stretchability, human-friendliness, and durability.<sup>[1,9]</sup>

In this Review, the recent developments in wearable and stretchable strain sensors are discussed. The materials compositions, fabrication process, and sensing mechanisms of resistive, capacitive, and optical sensors are studied in detail. The sensing performance of stretchable strain sensors in terms of stretchability, sensitivity, linearity, hysteresis, response and recovery time, overshoot effect, and dynamic durability is explored and compared. Finally, favorable applications of wearable strain sensors and current challenges are highlighted, and an outlook is presented. Unlike recent review papers focusing on a specific type of strain sensors,<sup>[11,21–26]</sup> this Review thoroughly covers all major types of wearable strain sensors, explicitly categorizes strain sensing parameters, and gives a detailed sensing comparison among recently reported wearable strain sensors. Compared with our previous Feature article,<sup>[1]</sup> this article further reviews optical and textile-based stretchable strain sensors and comprehensively discusses potential applications of wearable and stretchable strain sensors.

## 2. Classification of Stretchable Strain Sensors

Resistive, capacitive, piezoelectric, triboelectric, and optical strain sensors are the most explored stretchable strain sensors. Among them, piezoelectric and triboelectric strain sensors usually operate under high frequencies and cannot capture the static strain because of the fast charge transfer.<sup>[27]</sup> Therefore, their practical use in multiscale and wearable strain sensing is still questionable. On the other hand, resistive- and capacitive-type strain sensors have been extensively studied in recent years for wearable and skin-mountable strain sensing applications given their relatively simple readout, high stretchability, acceptable dynamic performance, and facile fabrication process (Figure 1).<sup>[1,11,37]</sup> Recently, soft and stretchable optical strain sensors have also received considerable interest in wearable and soft robotic applications because of their merits, such as resistance to environmental factors (e.g., temperature and humidity) and minimized sensitivity to electromagnetic interference (Figure 1).<sup>[28,38,39]</sup> In view of the above statements, this Review only emphasizes resistive, capacitive, and optical strain sensors.

### 2.1. Resistive-Type Strain Sensors

The resistive-type strain sensors based on metal foils were initially introduced in the early 1940s and have been exploited for the detection of limited strains up to 5%, such as small deformations in composites and rigid bodies.<sup>[37,40]</sup> Nowadays, the demand for wearable electronic devices has changed the structure of resistive-type strain sensors from brittle to stretchable format. Stretchable strain sensors are typically composed of active sensing materials combined with flexible and stretchable supporting substrates.<sup>[40,41]</sup> The active materials are usually in the forms of conducting micro-/nanomaterials–polymers



**Hamid Souri** received his B.Sc. degree in mechanical engineering from Sharif University of Technology, Iran, in 2012, and his M.Sc. degree in civil and environmental engineering from KAIST, South Korea, in 2015. He obtained his Ph.D. in mechanical engineering at the University of Auckland, New Zealand, in 2019. He is currently a project engineer at Aroa Biosurgery Limited, New Zealand. His research interests include flexible electronic devices for healthcare, smart materials, and composite materials.



**Metin Sitti** is the director of Physical Intelligence Department at the Max Planck Institute for Intelligent Systems in Stuttgart, Germany, since 2014. He received a Ph.D. degree in electrical engineering from the University of Tokyo, Japan, in 1999. He was a research scientist at University of California at Berkeley, USA between 1999 and 2002, and a professor at Carnegie Mellon University, USA, from 2002 to 2016. His research interests include small-scale physical intelligence, mobile milli-/microrobots, bioinspiration, advanced soft functional materials, and miniature medical robots.



**Morteza Amjadi** received his B.Sc. and M.Sc. degrees from Iran University of Science and Technology (IUST), Iran, and Korea Advanced Institute of Science and Technology (KAIST), South Korea, in 2012 and 2014, respectively. He obtained his Dr.Sc. degree jointly from Max Planck Institute for Intelligent Systems, Germany, and ETH Zurich, Switzerland. He is currently an assistant professor at Heriot-Watt University, UK. His research interests include wearable medical devices, smart materials, composites, and soft robotics.

composites, thin films, or conductive yarns/fabrics. In fact, the conductive network of active materials serves as a resistor under an applied voltage. When stretched/compressed, the electrical resistance of the conductive network changes as a function of the applied mechanical strain. The resistance variations upon stretching originate from geometrical changes (i.e., length and cross-sectional area), intrinsic resistive response of active materials, tunneling effect, and/or disconnection mechanism.<sup>[1,37,40]</sup> After releasing strain sensors from tensile/compressive strains, the resistance recovers to its initial values in a reversible manner. Thus, the deformation state can be readily measured by recording changes in the electrical resistance of resistive-type strain sensors.

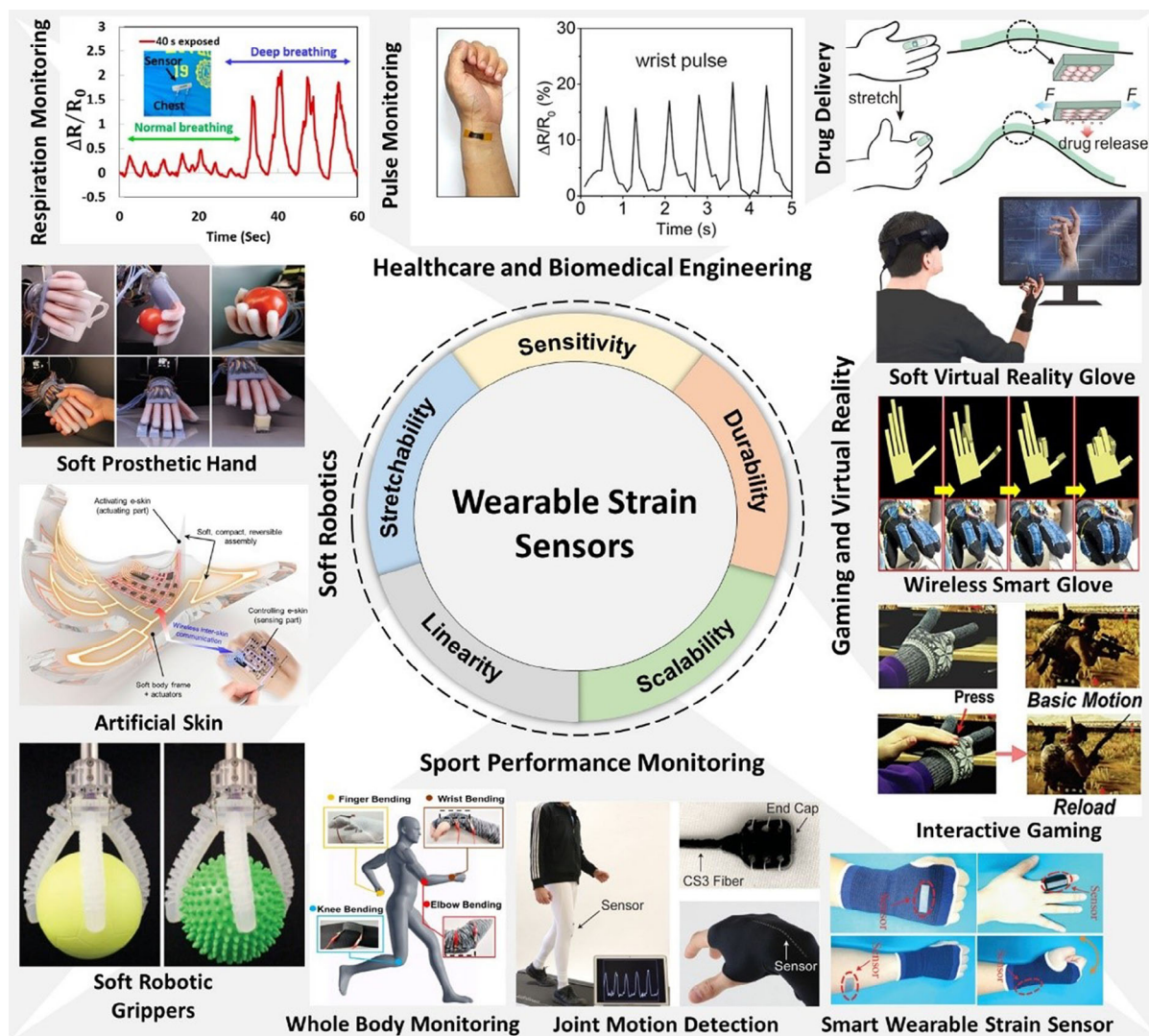


**Figure 1.** Wearable and stretchable strain sensors and their potential applications in healthcare and biomedical engineering, sport performance monitoring, soft robotics, and gaming and virtual reality. Soft prosthetic hand. Reproduced with permission.<sup>[28]</sup> Copyright 2016, American Association for the Advancement of Science. Soft robotic gripper. Reproduced with permission.<sup>[29]</sup> Copyright 2018, Wiley-VCH. Joint motion detection. Reproduced with permission.<sup>[30]</sup> Copyright 2015, Wiley-VCH. Smart wearable strain sensor. Reproduced with permission.<sup>[31]</sup> Copyright 2017, Royal Society of Chemistry. Wireless smart glove. Reproduced with permission.<sup>[8]</sup> Copyright 2014, American Chemical Society. Soft virtual reality glove. Reproduced with permission.<sup>[32]</sup> Copyright 2019, Springer Nature. Pulse monitoring. Reproduced with permission.<sup>[33]</sup> Copyright 2016, American Chemical Society. Respiration monitoring. Reproduced with permission.<sup>[6]</sup> Copyright 2016, American Chemical Society. Whole body monitoring. Reproduced with permission.<sup>[34]</sup> Copyright 2018, American Chemical Society. Drug delivery. Reproduced with permission.<sup>[7]</sup> Copyright 2015, American Chemical Society. Artificial skin. Reproduced with permission.<sup>[35]</sup> Copyright 2018, American Association for the Advancement of Science. Interactive gaming. Reproduced with permission.<sup>[36]</sup> Copyright 2019, Wiley-VCH.

## 2.2. Capacitive-Type Strain Sensors

Wearable capacitive-type strain sensors are often fabricated by sandwiching an insulating film known as a dielectric layer between two stretchable electrodes.<sup>[1]</sup> Under an applied voltage, the accumulated opposite charges on each electrode cannot flow through the dielectric layer, yielding a capacitor with an initial capacitance of  $C_0$ , which is expressed as

$$C_0 = \epsilon_0 \epsilon_r G \quad (1)$$

where  $\epsilon_0$  is the permittivity of air,  $\epsilon_r$  represents the dielectric constant of the dielectric material, and  $G$  is a function of the capacitor's geometry. For example, the initial capacitance for a parallel-plate capacitor can be calculated as

$$C_0 = \epsilon_0 \epsilon_r \frac{A_c}{d} \quad (2)$$

where  $A_c$  denotes the overlapped area of electrodes, and  $d$  is the thickness of the dielectric layer. The capacitance of strain sensors, which is independent of the resistance value of the

electrodes, increases under stretching due to the geometrical changes in the capacitive area.<sup>[1,23]</sup>

### 2.3. Optical Strain Sensors

Wearable optical strain sensors are typically composed of a stretchable waveguide with a core-cladding structure flanked by light emitter and photodetector. Since the introduction of novel fabrication techniques in electronics (e.g., soft lithography and 3D printing), flexible polymeric waveguides have been investigated for wearable strain sensing applications.<sup>[20,28,38]</sup> The principal sensing mechanism is based on the changes in the transmission of strain sensors upon deformation measured by the generated light power difference between the light source and photodetector.<sup>[28]</sup> The most recently reported stretchable optical strain sensors have shown promising results in terms of resolution and dynamic performance.<sup>[20,42]</sup>

### 2.4. Other Types of Stretchable Strain Sensors

As aforementioned, other types of stretchable strain sensors have also been developed in the past decade. Piezoelectric and triboelectric strain sensors are the two major types of stretchable strain sensors.<sup>[43–49]</sup> Piezoelectricity is a mechanism in which the electrical voltage is directly generated under external deformation due to the electrical dipole moments in piezoelectric materials.<sup>[50]</sup> Strain sensors based on active materials with a high piezoelectric coefficient can detect mechanical deformations with high sensitivity and fast response.<sup>[50]</sup> Wearable triboelectric strain sensors have been introduced more recently. They work based on the conversion of external deformations into electricity by the conjunction of the triboelectric effect and electrostatic induction. Moreover, when two thin materials with opposite triboelectricity contact each other, the charge transfer at their interface results in the creation of output potential.<sup>[50]</sup> The amount of the generated potential is as a function of the interaction with the source of external load/deformation that determines the contact conditions such as time and area. For further information regarding flexible and stretchable piezoelectric and triboelectric sensing devices, the reader is referred to the following reviews.<sup>[22,47,51]</sup>

## 3. Strain Sensing Materials

A crucial step in the design of stretchable strain sensors is the selection of appropriate materials, assembled structures, and fabrication methods. Various conductive materials including carbon nanomaterials (e.g., carbon blacks [CBs], carbon nanotubes [CNTs], graphene and its derivatives),<sup>[6,9,34,52–70]</sup> metal nanowires (NWs), nanofibers (NFs), and nanoparticles (NPs),<sup>[8,16,71–79]</sup> MXenes (e.g.,  $Ti_3C_2T_x$ ),<sup>[10,80,81]</sup> ionic liquid,<sup>[82,83]</sup> hybrid micro-/nanostructures,<sup>[84–96]</sup> and conductive polymers<sup>[97–101]</sup> have been utilized as active sensing materials. Regardless of the type of stretchable strain sensors, the active materials have been incorporated into stretchable supporting materials such as silicone elastomers (e.g., Ecoflex and polydimethylsiloxane [PDMS]),<sup>[6,8–10,16,31,52,56,59,65,67,69,70,73–75,82,85,87–89,91,92,95,96,102–130]</sup>

rubbers,<sup>[55,57,66,76,81,94,131–135]</sup> thermoplastic polymers,<sup>[54,58,63,64,68,80,84–86,99,136–140]</sup> and medical adhesive films.<sup>[33,141,142]</sup> Natural fiber-based materials such as cotton, wool, and flax have also been widely used as supporting substrates for the fabrication of stretchable strain sensors.<sup>[143–150]</sup> Thermoplastic polyurethane (TPU),<sup>[28]</sup> polystyrene-based elastomers,<sup>[38]</sup> and PDMS<sup>[20,151]</sup> are examples of materials used in stretchable optical strain sensors. The appropriate choice of conductive nanomaterials and their interaction with stretchable supporting materials greatly affect the sensing properties of stretchable strain sensors, which will be further discussed in the following sections. **Figure 2** shows the examples of stretchable, wearable, and skin-mountable strain sensors. Such strain sensors can be directly attached to highly deformable and irregular surfaces for continuous strain monitoring without any slippage or delamination from the target object.

## 4. Fabrication of Wearable Strain Sensors

Low-cost, facile, reliable, and scalable manufacturing strategies are highly desirable for the large-scale production of wearable strain sensors. To date, different fabrication techniques including chemical synthesis, electrospinning, coating and sputtering, printing, transfer patterning, liquid-phase blending, filtration, and laser micromachining have been proposed for the fabrication of polymer-based strain sensors. **Figure 3a** shows the fabrication process of highly sensitive strain sensors composed of one-step chemical vapor deposition (CVD)-grown freestanding graphene woven fabrics (GWFs) transferred onto the PDMS substrate.<sup>[126]</sup> The electromechanical characterizations of the GWFs-PDMS strain sensors under various growth conditions and GWFs orientation were investigated. Huang et al. reported wearable strain sensors based on parallelly aligned vertical graphene (PAVG) sheets and PDMS composites (**Figure 3b**).<sup>[52]</sup> The PAVG sheets were synthesized via the inductively coupled plasma CVD (ICPCVD) process and were then transferred to the PDMS film. In another approach, Wang et al. reported resistive-type stretchable strain sensors based on the conductive network of reduced graphene oxide (rGO) decorated on the TPU electrospun fibrous mats (**Figure 3c**).<sup>[64]</sup> The ultrasound-assisted coating of rGO sheets on the surface of TPU fibers resulted in a 3D conductive structure with tunable sensing properties. **Figure 3d** shows layer-by-layer spray coating of  $Ti_3C_2T_x$  MXene and CNTs on an elastic latex rubber film, yielding highly stretchable strain sensors.<sup>[81]</sup> Guo et al. developed highly elastic sandwich structured strain sensors based on the synergistic conductive network of the CNTs/CBs hybrid film spin-coated over the PDMS substrate.<sup>[92]</sup> The 3D printing process has been used to develop stretchable strain sensors made of chemically prepared CNTs/graphene oxide (GO) composite dough.<sup>[153]</sup> In another work, Wang et al. reported fully 3D-printed stretchable strain sensors using TPU/silver (Ag) microflake composite as an electrode layer, PDMS as supporting substrate, and TPU/CBs/sacrificial NaCl template as sensing layer.<sup>[139]</sup> This novel structure minimized inplane stretching disturbance, thereby leading to customizable stretchable strain sensors. A stretchable strain sensor has been reported by line-patterning of vertically aligned CVD-grown CNT bundles followed by their rolling and transferring

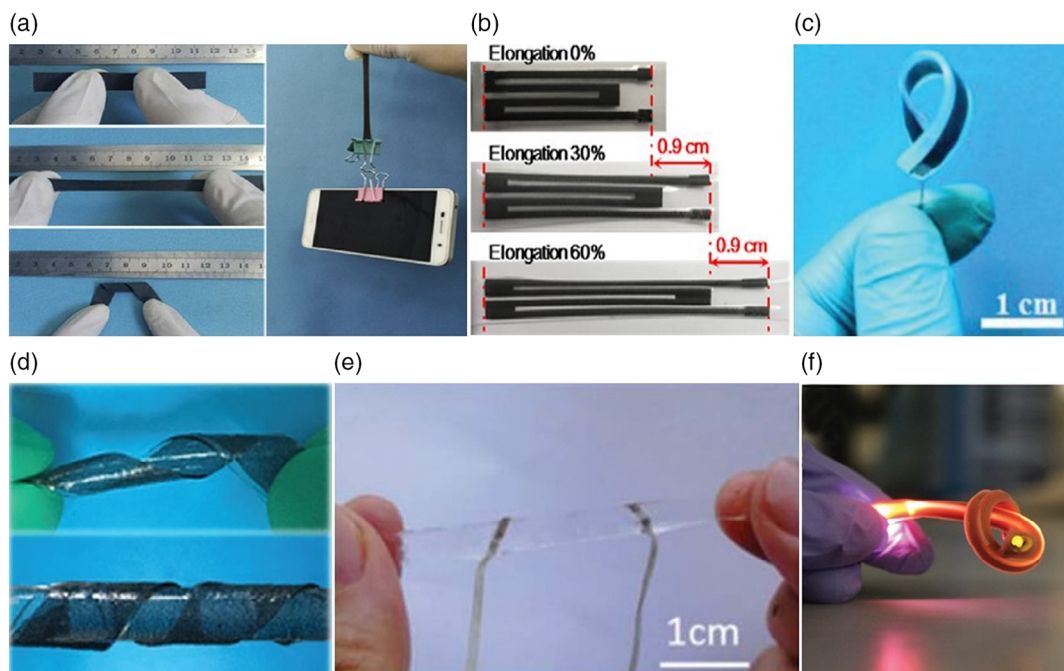


**Figure 2.** Photographs of stretchable, wearable, and skin-mountable strain sensors. a) A stretchable strain sensor based on the rGO/TPU composite. Reproduced with permission.<sup>[64]</sup> Copyright 2018, Elsevier. b) A serpentine-shaped strain sensor based on the Ecoflex elastomer embedded with graphite films. Reproduced with permission.<sup>[104]</sup> Copyright 2018, Elsevier. c) A strain sensor made of the carbonized cotton fabric sandwiched between Ecoflex layers. Reproduced with permission.<sup>[148]</sup> Copyright 2016, Wiley-VCH. d) Stretchable strain sensors made of the carbonized silk georgette and PDMS composite. Reproduced with permission.<sup>[152]</sup> Copyright 2017, Royal Society of Chemistry. e) An ultrastretchable capacitive-type strain sensor based on the metal NFs-ionic hydrogels nanocomposite. Reproduced with permission.<sup>[71]</sup> Copyright 2019, Royal Society of Chemistry. f) A flexible and highly stretchable optical strain sensor based on the TPU/silicone fiber. Reproduced with permission.<sup>[28]</sup> Copyright 2016, American Association for the Advancement of Science.

onto the silicone elastomer substrate (Figure 3e).<sup>[56]</sup> In another approach, highly stretchable strain sensors have been fabricated based on rGO/deionized water (DI) solution filled in Ecoflex channels via a simple template method.<sup>[65]</sup> Shi et al. reported highly sensitive and wearable strain sensors made of a composite film containing graphene NPs (GNPs) and PDMS.<sup>[66]</sup> A medical tape was used to transfer the GNP film onto the patterned PDMS substrates by mechanical pressing, resulting in highly conductive networks (surface resistance of  $20\text{--}30\ \Omega\ \text{sq}^{-1}$ ) for strain sensing. Interface-controlled conductive fibers made of Ag NWs and TPU composite were developed for wearable sensing applications.<sup>[121]</sup> The effect of the bonding layer between Ag NWs and TPU fibers on the sensing performance of wearable strain sensors were investigated. A capacitive-type strain sensor has been reported based on the wrinkled PDMS dielectric layer.<sup>[13]</sup> The thermally evaporated gold (Au) film on parylene electrodes was then transferred onto the PDMS layer to construct the strain sensor. The authors have shown improvements in the electromechanical performance of the strain sensor when the thickness of electrodes was controlled at the nanoscale. Laser direct writing (LDW) has been recently introduced as an effective and scalable process for the manufacturing of wearable sensors.<sup>[154–158]</sup> For instance, LDW was used to develop stretchable strain sensor arrays by turning Ecoflex elastomer into silicon carbide conductive patterns through the localized laser irradiation.<sup>[158]</sup>

Apart from the polymeric supporting materials, natural fibers, yarns, and fabrics have been activated by conductive

materials through techniques such as carbonization process, dip-coating, bar coating, ultrasonication, and vacuum filtration.<sup>[23,143–150,152,159–163]</sup> Carbonization is a well-established process where carbonaceous substances such as natural fibers are broken down into elemental carbon and chemical compounds by heating (Figure 4a).<sup>[148,149]</sup> During the carbonization process, natural fiber-based materials are heated up in a vacuum oven in the presence of an inert gas without any oxygen from the air, converting them into electrically conductive active materials for strain sensing. Modal fabrics,<sup>[161]</sup> cotton fabrics,<sup>[148]</sup> and silk fabrics<sup>[149,152]</sup> have been successfully carbonized to develop free-standing conductive structures. These active materials were then combined with elastomers to manufacture stretchable strain sensors. Despite advancements in the carbonization method, its disadvantages are costly equipment requirements (e.g., vacuum furnaces), multistep and time-consuming process, high energy consumption, and limitations for large-scale productions.<sup>[144,146]</sup>

The dip-coating of conductive yarns/fabrics in conductive inks is the most common coating technique for their activation. As an example, dip-coated wool yarns and cotton fabric in the hybrid ink of GNPs and CBs were encapsulated with the Ecoflex elastomer to construct stretchable strain sensors (Figure 4b).<sup>[143,145]</sup> In another study, a two-step dip-coating process was utilized to fabricate stretchable strain sensors based on cotton fabric.<sup>[162]</sup> The cotton fabric was first dip-coated with GO followed by the reduction process. Then, the rGO coated cotton fabric was dip-coated in a CNT ink to improve the conductivity of the cotton

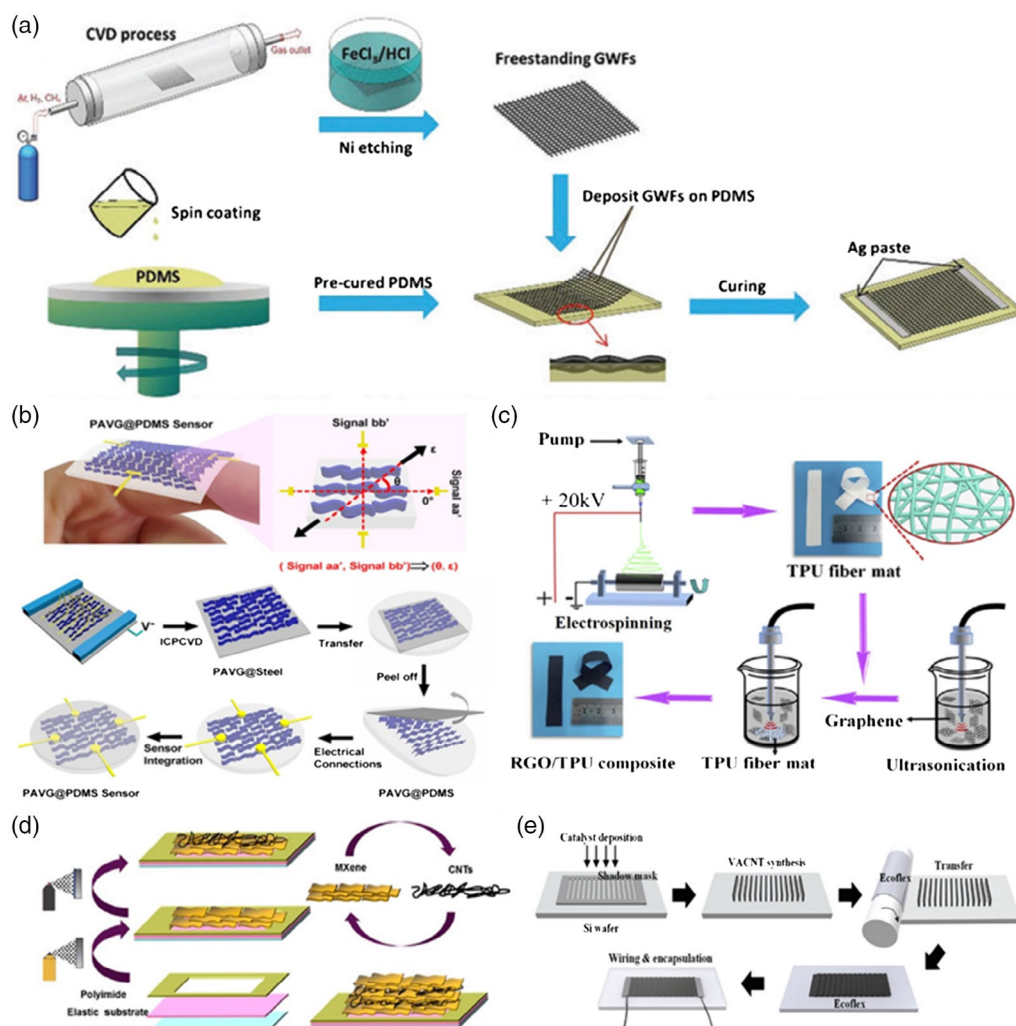


**Figure 3.** Fabrication processes of stretchable polymer-based strain sensors. a) Fabrication of GWFs-based stretchable strain sensors. Reproduced with permission.<sup>[126]</sup> Copyright 2017, Royal Society of Chemistry. b) Fabrication procedure of the PAVG-based strain vector sensors through ICPCVD process. Reproduced with permission.<sup>[52]</sup> Copyright 2019, American Chemical Society. c) Fabrication of rGO/TPU electrospun fibrous mat strain sensors. Reproduced with permission.<sup>[64]</sup> Copyright 2018, Elsevier. d) Layer-by-layer spray coating of a sandwich-like  $\text{Ti}_3\text{C}_2\text{T}_x$  MXene/CNTs strain sensing film. Reproduced with permission.<sup>[81]</sup> Copyright 2018, American Chemical Society. e) Fabrication process of strain sensors based on vertically aligned CNTs encapsulated with Ecoflex elastomer. Reproduced with permission.<sup>[56]</sup> Copyright 2019, Wiley-VCH.

fabrics. Cataldi et al. fabricated highly conductive ( $\approx 10 \Omega \text{sq}^{-1}$ ) cotton fabric nanocomposites through spray coating of graphene-TPU dispersions and subsequent hot pressing.<sup>[147]</sup> The nanocomposites showed stability to various mechanical folding-unfolding and washing cycles, making them ideal for wearable sensing applications. Souri and Bhattacharyya have achieved highly conductive flax yarns by ultrasonication coating technique using a simple ultrasonic bath and GNPs-CBs hybrid materials.<sup>[144]</sup> Later, conductive cotton and wool fabrics were developed using a scaled-up ultrasonication coating.<sup>[146]</sup> Highly stretchable sandwich-structured strain sensors were fabricated by the encapsulation of the conductive fabrics within the Ecoflex elastomer. Vacuum infiltration of the GO dispersion through cotton fabric followed by hot-pressing reduction was also used to fabricate strain sensors with good washing stability.<sup>[159]</sup> It is noted that most of the developed natural

fiber-based strain sensors are resistive-type sensors. This could be due to the complex and hierarchical structure of conductive fiber materials, making them suitable for highly sensitive strain sensing. In a recent study, Atalay et al. also reported a capacitive-type strain sensor composed of a porous dielectric layer and soft conductive fabric as stretchable electrodes.<sup>[164]</sup>

Stretchable optical sensors have been fabricated from optically transparent polymeric materials such as hydrogels and elastomers.<sup>[19,20,28,38,151,165,166]</sup> Figure 5a shows the coextrusion process to develop stretchable thermoplastic elastomer optical fibers.<sup>[38]</sup> The setup was based on two single-screw extruders that fed the polymeric melt (a polystyrene-based elastomer as the core material and a fluorinated polymer as cladding) into a concentric coextrusion nozzle to form the core-cladding structure. The fibers were then naturally cooled down and collected by a spool.

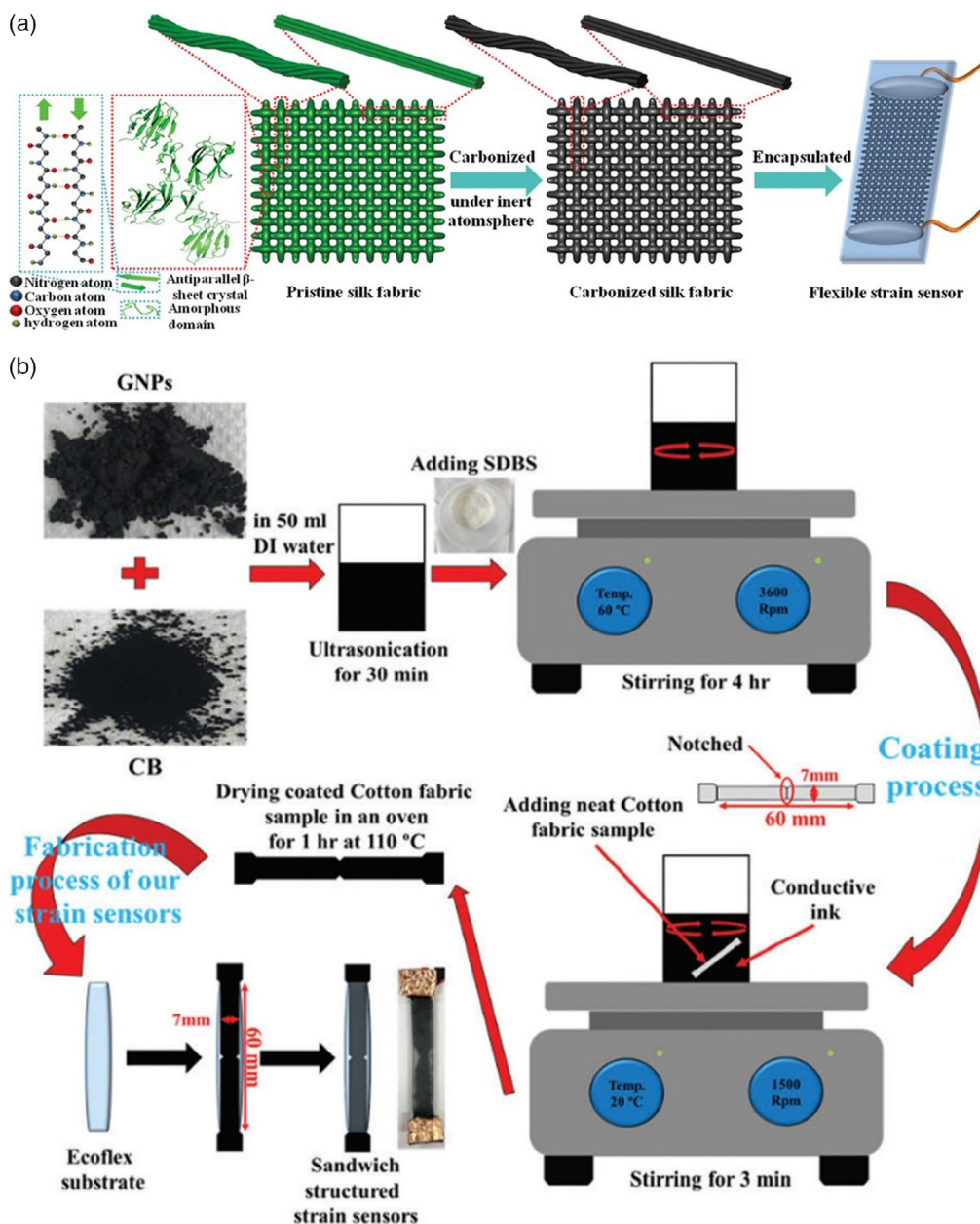


**Figure 4.** Fabrication of stretchable strain sensors based on conductive natural yarns/fabrics. a) Carbonization process for the manufacturing of carbonized silk fabric-based stretchable strain sensors. Reproduced with permission.<sup>[149]</sup> Copyright 2016, Wiley-VCH. b) Fabrication procedure of GNPs-/CBs-coated cotton fabric strain sensors.<sup>[145]</sup> Copyright 2018, Royal Society of Chemistry.

Alternatively, a two-step process was used to fabricate Au NP-loaded PDMS optical fibers in a core/cladding step-index structure (Figure 5b).<sup>[20]</sup> The liquid PDMS containing Au NPs was first injected in a tube mold, cured, and finally ejected by water pressure. The resulted core was then coated with the pure PDMS cladding layer by dip- and spin-coating. In a similar approach, Gou et al. developed a hydrogel fiber-based highly stretchable optical strain sensor.<sup>[165]</sup> The hydrogel precursor was injected into a silicone tube mold and cured. The core was then ejected and dipped into the Na-alginate-polyacrylamide precursor to form a clad-coated core optical fiber. In another method,

Qu et al. manufactured multimaterial optical and electronic fibers using a thermal drawing scalable approach (Figure 5c).<sup>[166]</sup> The macroscopic preform of optical fibers was first machined, and the assembly was then thermally drawn, yielding kilometer-long multimaterial optical fibers for strain sensing.

## 5. Strain Sensing Mechanisms

This section details different strain sensing mechanisms of resistive, capacitive, and optical strain sensors. The principal

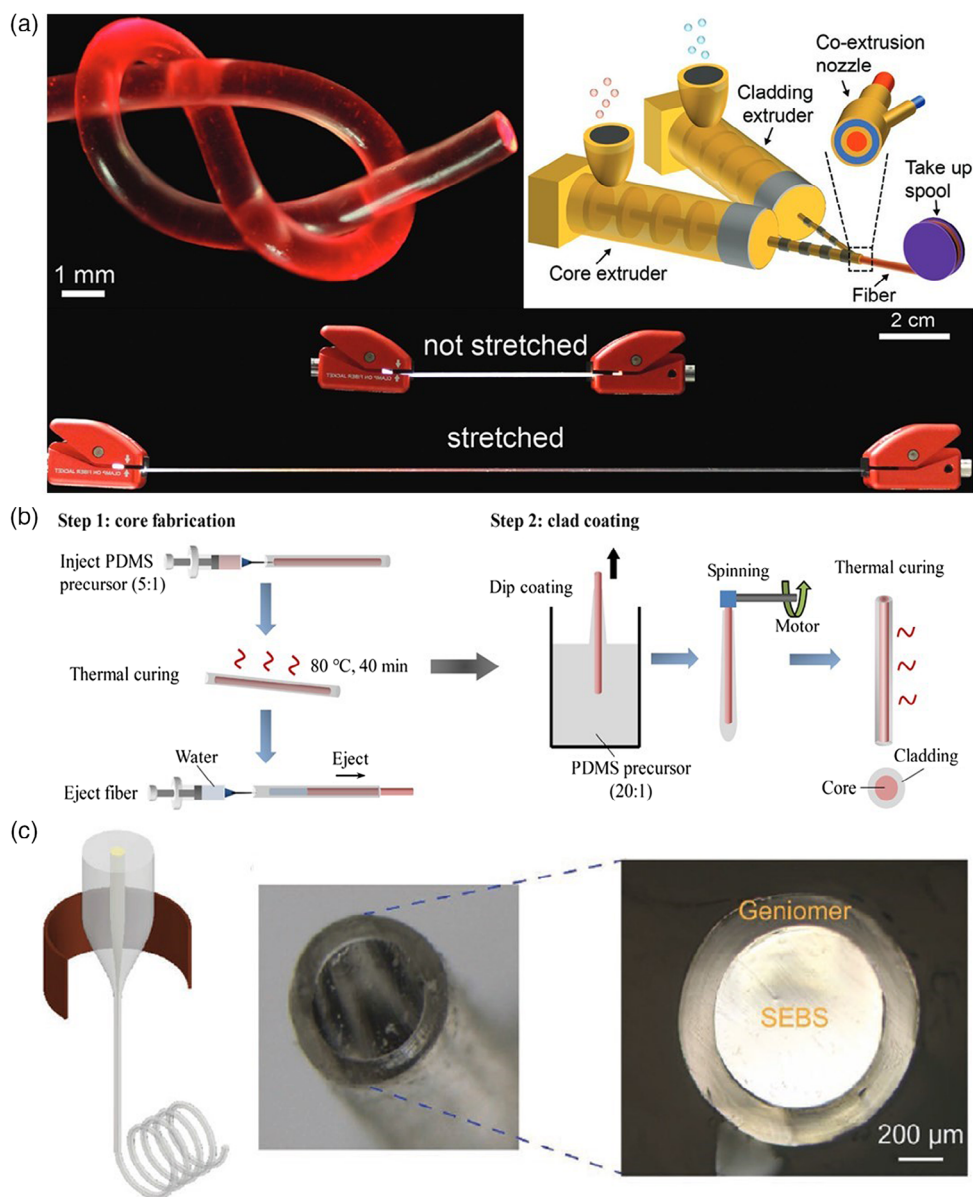


**Figure 5.** Fabrication of stretchable optical strain sensors. a) Coextrusion process of the stretchable thermoplastic elastomer optical waveguides. Reproduced with permission.<sup>[38]</sup> Copyright 2018, Wiley-VCH. b) Two-step fabrication of stretchable optical fibers with a core/cladding step-index structure. Reproduced with permission.<sup>[20]</sup> Copyright 2019, American Chemical Society. c) Fabrication of superelastic multimaterial optical fibers composed of a core poly(styrene-*b*-(ethylene-*co*-butylene)-*b*-styrene) (SEBS) copolymer and a Geniomer cladding via thermal drawing. Reproduced with permission.<sup>[166]</sup> Copyright 2018, Wiley-VCH.

sensing mechanism for capacitive-type and optical sensors is their dimensional changes upon stretching. In addition to the intrinsic resistive response of materials themselves and geometrical effects, stretchable resistive-type strain sensors have been successfully developed by the disconnection of micro-/nanomaterials, tunneling effect, and creation of controlled microcracks in the sensing film. These mechanisms tune the electromechanical response of stretchable strain sensors, depending on the type of sensing materials, their surface interaction with supporting materials, and the fabrication process.<sup>[1]</sup>

### 5.1. Geometrical Effect

The cross-sectional area of materials changes upon stretching due to their Poisson's ratio. The resistance of resistive-type strain sensors can be altered with respect to the variations in their length and cross-sectional area during external stretching/releasing cycles as below<sup>[1]</sup>

$$R = \rho \frac{L}{A_r} \quad (3)$$



where  $L$  is the length of sensors,  $A_r$  is the cross-sectional area of conductive sensing films, and  $\rho$  is the electrical resistivity of the sensing materials. The dominant working principle of the liquid metal-based stretchable strain sensors is the geometrical effect.<sup>[167–171]</sup> In the following sections, it will be shown that the contribution of this mechanism to the overall sensing performance of nanomaterials-based stretchable sensors may not be significant.

The geometrical effect plays a key role in controlling the strain sensing properties of capacitive and optical fiber strain sensors.<sup>[1,28]</sup> When a capacitive-type strain sensor with the respective length, width, and dielectric thickness of  $l_0$ ,  $w_0$ , and  $d_0$  is stretched by a strain of  $\epsilon$ , the length of the strain sensor increases to  $(1 + \epsilon)l_0$ , whereas the width and thickness decline to  $(1 - \nu_{\text{electrode}}\epsilon)w_0$  and  $(1 - \nu_{\text{dielectric}}\epsilon)d_0$ . Therefore, the capacitance of the sensor upon stretching can be derived as

$$\begin{aligned} C &= \epsilon_0 \epsilon_r \frac{(1 + \epsilon)l_0(1 - \nu_{\text{electrode}}\epsilon)w_0}{(1 - \nu_{\text{dielectric}}\epsilon)d_0} = \epsilon_0 \epsilon_r \frac{(1 + \epsilon)l_0w_0}{d_0} \\ &= \epsilon_0 \epsilon_r \frac{(1 + \epsilon)A_0}{d_0} = (1 + \epsilon)C_0 \end{aligned} \quad (4)$$

It is noted that  $\nu_{\text{electrode}}$  and  $\nu_{\text{dielectric}}$  are assumed equal, given the thin nature of stretchable electrodes and softness of both electrode and dielectric layers.<sup>[1]</sup> Based on the aforementioned equation, changes in the capacitive area, as well as the thickness of the dielectric layer, lead to the shift of the capacitance as a function of the external deformation (stretching or compression).

The strain sensing principle of stretchable optical sensors relies on the attenuation in the light transmission when the stretchable optical waveguides are stretched.<sup>[28,39,151]</sup> The absorbance of a waveguide with the length of  $L$  can be derived from the Beer–Lambert law<sup>[28]</sup>

$$A = ecL \quad (5)$$

where  $A$  is the absorbance,  $e$  is the absorptivity of the optical material, and  $c$  is the concentration of chemical species in the medium that attenuate light. When the waveguide is stretched to  $\epsilon$  ( $\epsilon = \frac{L-L_0}{L_0}$ ), its absorbance can be obtained from<sup>[28]</sup>

$$A = \frac{a}{10} + A_0 \quad (6)$$

where  $a$  is the output power loss, and  $A_0 = ecL_0$  is the baseline absorbance. Assuming that  $e$  and  $c$  are constant during stretching, the output power loss of the waveguide is expressed as

$$a = 10ecL_0\epsilon \quad (7)$$

The aforementioned equation reveals a linear relationship between the output power loss of stretchable optical sensors and the applied strain. For further details about the working mechanism of other types of optical strain sensors (e.g., diffraction grating, photonic crystal, and surface plasmon sensors), we refer the reader to the following review paper.<sup>[39]</sup>

## 5.2. Intrinsic Resistive Response of Materials

One of the most commonly used sensing principles in both traditional resistive-type strain gauges and newly developed

stretchable strain sensors is the intrinsic resistive response of the sensing materials. This effect is defined as the change in the electrical resistance of a material in response to external deformations, and is the fundamental mechanism of semiconductor (e.g., silicon and germanium)-based strain sensors. Upon the mechanical deformation, the resistance of sensors dramatically increases due to the change in the bandgap on interatomic spacing.<sup>[23,37,40]</sup> Semiconducting CNTs and oxide NWs (e.g., zinc oxide NWs) bear ultrahigh resistive response, which resulted in the development of highly sensitive strain sensors by their incorporation into highly stretchable substrates.<sup>[1,23,41]</sup> Nevertheless, large mechanical mismatch and weak interfacial adhesion between micro-/nanoscale materials and stretchable supporting materials dramatically lower the contribution of their intrinsic resistive response to the overall sensing performance of stretchable strain sensors.<sup>[1,11]</sup>

## 5.3. Disconnection Mechanism

In resistive-type strain sensors, the strain sensing behavior can be attributed to the changes in the conduction network upon stretching/releasing loads.<sup>[23]</sup> Based on the percolation theory, there is a threshold for the minimum number of nanomaterials to establish conducting paths within a film or composite. When the adjacent nanomaterials are connected, electrons can pass through the established conducting network.<sup>[1,40,41]</sup> Upon stretching the resistive-type strain sensors, some of these nanomaterials lose their overlapped area and electrical connection, thereby increasing the overall electrical resistance of strain sensors. The disconnection originates from large stiffness mismatch between nanomaterials and stretchable supporting materials, leading to the slippage and debonding of nanomaterials upon large stretching. Stretchable strain sensors based on NWs and flakes particularly take advantage of the disconnection mechanism.<sup>[1,8,37,55,57,144,172]</sup> For instance, the resistance shift in stretchable strain sensors made of  $\text{Ti}_3\text{C}_2\text{T}_x$  MXene/CNTs films coated over the latex substrate was reported to be due to the changes in the overlapping areas and interconnecting pathways during cyclic stretching-releasing.<sup>[81]</sup> Similar behavior has been observed in the conductive network of Au nanosheets dropcast on the Ecoflex substrate.<sup>[118]</sup> Upon stretching, the nanosheets slip toward the direction of the external load, decreasing the contact area between them and thus increasing the overall resistance of the strain sensor.

## 5.4. Crack Generation in Conductive Films

The cracks appear and propagate in brittle thin films coated over the top surface of soft polymers or natural fibers upon stretching due to their mechanical mismatch with the supporting materials. Cracks intend to initiate at the stress-concentrated areas. Although cracks are undesirable for structural designs, the generation of microcracks in conductive thin films has been successfully utilized to develop highly sensitive strain sensors. The opening and enlargement of microcracks have been observed in CNT-based strain sensors,<sup>[109,138,173,174]</sup> graphene-based strain sensors and its derivatives,<sup>[6,57,117]</sup> metal NW- and NPs<sup>[86,116,175–180]</sup> based strain sensors. The rapid separation of nanomaterials

at the microcrack edges dramatically limits the electrical conduction paths within the thin films, leading to a significant increase in the electrical resistance of strain sensors under the applied tensile strain.<sup>[1,6]</sup> Most recently, controlled crack propagation has been used as an effective mechanism to greatly promote the sensitivity of stretchable sensitive strain sensors.<sup>[6,116,145,179]</sup> For instance, a strain sensor based on the cut-through channel cracks of the Au thin film on PDMS substrate was fabricated, and the effect of the channel cracks on the sensitivity and electromechanical response were explored.<sup>[116]</sup> Amjadi et al. fabricated ultrasensitive and stretchable strain sensors based on the controllable and reversible parallel microcracks in graphite films bar coated over the plasma-exposed Ecoflex elastomer (**Figure 6a**).<sup>[6]</sup> The length and density of microcracks were increased by the applied strain, and microcrack edges were reconnected upon releasing, ensuring the recovery of the electrical resistance after the complete strain release. In natural fiber-based strain sensors, the fiber breakage in the direction of the applied strain leads to the crack propagation and subsequent increase in electrical resistance.<sup>[145,146,148]</sup> Researchers have fabricated natural fiber strain sensors with high sensitivity and stretchability based on controlled crack propagation and fiber breakage (**Figure 6b**).<sup>[145,148,149,152]</sup>

### 5.5. Tunneling Effect

Tunneling occurs when electrons pass through a nonconductive material filled between closely distanced conductive

nanomaterials.<sup>[1,9]</sup> Conductive nanocomposites made of functional nanomaterials and polymer matrices have not only direct electrical paths through connected nanomaterials but also tunneling conduction between adjacent nanomaterials.<sup>[1,11,37]</sup> The minimum distance in which electrons pass through the nonconductive barrier to creating quantum tunneling junctions is called cut-off distance. The cut-off distance depends on several factors, including the type of insulating material, conductive fillers, and processing parameters.<sup>[1]</sup> The tunneling resistance originated from the quantum electron junctions can be calculated via Simmon's theory<sup>[9]</sup>

$$R_{\text{tunnel}} = \frac{V}{AJ} = \frac{h^2 d}{Ae^2 \sqrt{2m\lambda}} \exp\left(\frac{4\pi d}{h} \sqrt{2m\lambda}\right) \quad (8)$$

where  $V$  denotes the electrical potential,  $J$  is the tunneling current density,  $A$  is the cross-sectional area of the tunneling junction,  $d$  represents the distance between adjacent nanomaterials,  $h$  is Planck's constant,  $e$  is the single-electron charge,  $m$  is the electron mass, and  $\lambda$  is the height of energy barrier for the nonconductive barrier. The dominant strain-responsive mechanism of the CNTs-based nanocomposite strain sensors arises from the changes in the tunneling resistance.<sup>[1,9,103,181]</sup> In nanocomposite strain sensors, CNTs are often entangled and self-folded within polymeric matrices. When stretched, entangled CNTs are more susceptible to unfold rather than sliding, leading to the changes in the tunneling resistance among neighboring CNTs.<sup>[9]</sup> It is

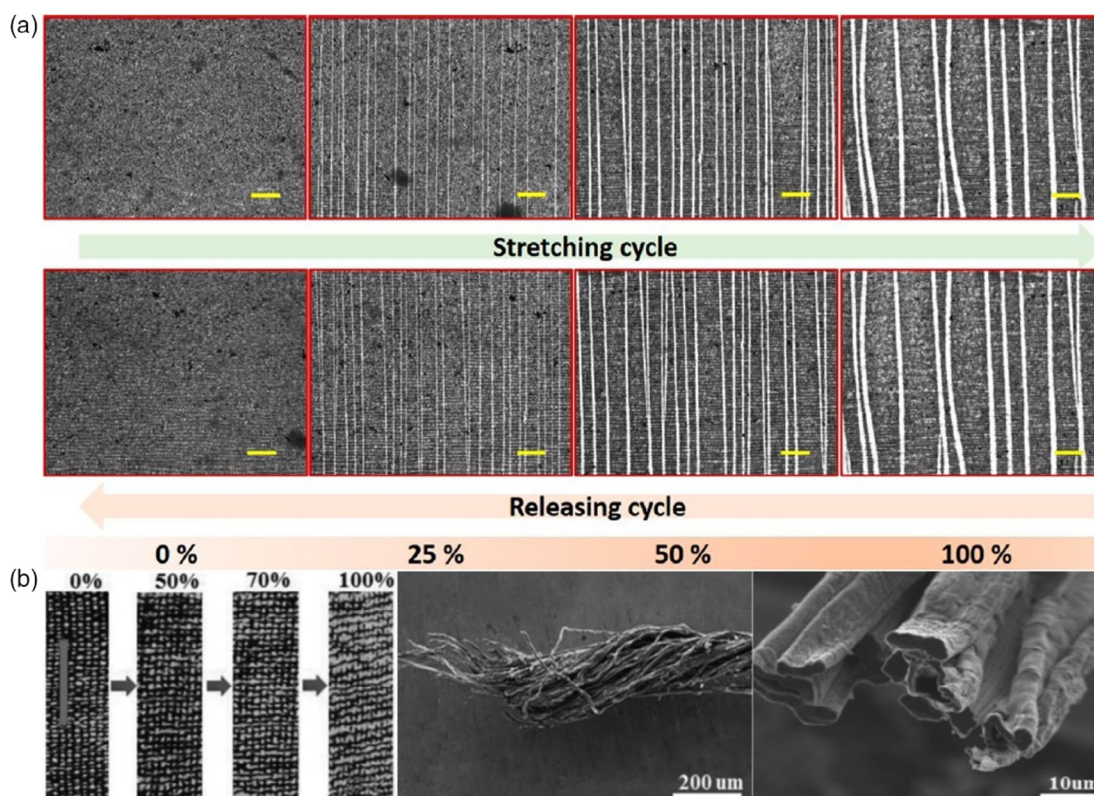


**Figure 6.** Crack generation in active materials coated over flexible supporting materials. a) Parallel microcrack opening in the graphite thin film coated on the Ecoflex substrate upon stretching. Reproduced with permission.<sup>[6]</sup> Copyright 2016, American Chemical Society. b) Photographs and microscopic images of a carbonized cotton strain sensor during stretching, resulting in fiber and yarn breakage. Reproduced with permission.<sup>[148]</sup> Copyright 2016, Wiley-VCH.

important to point out that the tunneling effect differs from the disconnection mechanism where many connected networks are separated due to the slippage of nanomaterials within polymer matrices.

## 6. Design Parameters for Stretchable Strain Sensors

The strain sensing performance of stretchable strain sensors can be fully characterized by design variables, including stretchability, sensitivity, linearity, hysteresis, response and recovery time, and dynamic durability. In this section, we compare the sensing parameters of the recently reported stretchable strain sensors.

### 6.1. Stretchability

The stretchability of a strain sensor reflects the maximum strain where the sensor maintains its physical integrity and response stability. This parameter mainly depends on the type of matrix or substrate, fabrication process, and the aspect ratio of micro-/nanomaterials used as sensing elements.<sup>[1]</sup> The stretchability of the recently reported strain sensors varies greatly from 2% to 1400% (Table 1 and 2). Figure 7a shows the electro-mechanical behavior of a highly stretchable strain sensor (stretchability  $\approx$ 500%) based on a polymer composite consisting of graphene, poly(acrylic acid) (PAA), and amorphous calcium carbonate (ACC).<sup>[141]</sup> In this composite, graphene nanosheets and calcium ions ( $\text{Ca}^{2+}$ ) formed a double crosslinkers with low stiffness that could play a key role in achieving high stretchability. Xu et al. reported an ultrastretchable capacitive-type strain sensor based on ionic hydrogels and conductive Ag NF nanocomposites as a dielectric layer and stretchable electrodes, respectively.<sup>[71]</sup> The high stretchability of the dielectric layer and robustness of the electrodes were the key parameters in the stability of the sensor even at strains as large as 1000%. In general, the stretchability of strain sensors enhances using 2D or 3D nanomaterials rather than 1D nanomaterials because of their higher aspect ratio, facilitating the formation of the robust percolation network under large strains (Table 1). For instance, strain sensors based on the high aspect ratio metal NWs (e.g., Ag NWs) and CNTs often possess high stretchability of over 50%. Some of the recent strain sensors based on conductive natural fibers/fabrics have also shown high stretchability (>100%).<sup>[145,146,148]</sup> For instance, carbonized plain weave silk and cotton fabrics sandwiched between two layers of Ecoflex have shown stretchability up to 500% and 140%, respectively.<sup>[148,161]</sup> Stretchable optical strain sensors based on thermoplastic elastomer,<sup>[38]</sup> graphene/PDMS nanocomposite fibers,<sup>[19]</sup> PDMS waveguides,<sup>[151]</sup> and TPU/silicone fibers<sup>[28]</sup> have demonstrated stretchability up to 300%, 150%, 100%, and 85%, respectively.

### 6.2. Sensitivity

The sensitivity of a strain sensor is quantified by the gauge factor (GF), which is defined as the ratio of the relative change of the output signal to the applied strain.<sup>[1,37]</sup> The GF value of stretchable strain sensors depends on various factors, including

sensing elements, microstructure, sensing mechanism, and fabrication process.<sup>[23,41]</sup> For resistive-type strain sensors, the corresponding GF is defined as  $\text{GF} = (\Delta R/R_0)/\epsilon$  where  $\Delta R/R_0$  is the relative change of resistance and  $\epsilon$  is the applied strain. A resistive-type strain sensor made of the fragmented CNT paper–PDMS composite showed an ultrahigh sensitivity up to  $10^7$  at 50% strain.<sup>[111]</sup> The high sensitivity was attributed to the separation of CNT networks in the cracked areas. In another study, Ma et al. developed highly stretchable and ultrasensitive (GF of 88 443 at 350% strain) strain sensors based on an open mesh structure made of the 3D-printed graphene and PDMS nanocomposites followed by plasma treatment, polyethyleneimine coating, and finally deposition and reduction of GO particles.<sup>[183]</sup> The high GF mainly originated from the sliding and disconnection of rGO at low strain range, whereas the open mesh structure could enhance the sensitivity at high strain levels.

The natural fiber-based resistive-type strain sensors have shown a wide range of GF values from 1.2 to 102 351 (Table 2).<sup>[143–145,148,149]</sup> It has been shown that the GF of natural fiber strain sensors can be controlled through geometric engineering (Figure 8a).<sup>[143]</sup> Moreover, the serpentine-shaped active materials exhibited lower sensitivity than a straight one due to the less increased displacement at the direction of the applied strain. In another work, a strain sensor based on the fragmented conductive cotton fabric–Ecoflex composite showed ultrahigh sensitivity up to 102 351 within the strain range of 342–400% (Figure 8b).<sup>[145]</sup>

Theoretically, the maximum achievable GF of capacitive-type strain sensors with the parallel-plate structure is 1 ( $\text{GF} = (\Delta C)/C_0\epsilon = ((1 + \epsilon)C_0 - C_0)/C_0\epsilon = 1$ ), meaning that most of the stretchable capacitive-type sensors have GFs smaller than this limit (GFs < 1).<sup>[1]</sup> For instance, a CBs–filled elastomer composite and silicone elastomer-based strain sensor showed high stretchability up to 500% with GFs up to 0.98.<sup>[53]</sup> The GF value of 0.82 has been reported for stretchable capacitive-type sensors using hollow elastomeric fibers filled with liquid metal networks.<sup>[185]</sup> Despite this theoretical limitation of capacitive-type sensors, some recent works have demonstrated the possibility of sensitivity enhancement ( $\text{GF} > 1$ ) through geometric engineering and novel materials formulation.<sup>[15,71]</sup> For instance, Nur et al. developed a capacitive-type strain sensor using a part of ultrathin wrinkled Au-film electrodes and achieved a GF of around 3 under 140% tensile strain (Figure 7b).<sup>[15]</sup> Another highly sensitive capacitive-type sensor has been reported using ionic hydrogels and Ag NFs nanocomposite as a dielectric layer and flexible anisotropic conductive film coated with Ag NFs as electrodes.<sup>[71]</sup> The strain sensor showed a high GF of 165 under the ultrahigh strain of 1000%. The incorporation of Ag NFs greatly improved the hydrogel–metal interface, hence incremented the sensitivity.

In wearable optical strain sensors, the sensitivity is quantified by the stretch-dependent output power loss of stretchable waveguides under mechanical deformations.<sup>[28]</sup> For example, the sensitivity of a fiber strain sensor based on the TPU core and a highly absorptive silicone composite cladding was around  $18.75 \text{ dB } \epsilon^{-1}$ .<sup>[28]</sup> The sensitivities of stretchable strain sensors made of thermoplastic elastomer and dye-doped PDMS optical fibers were around 10 and  $3.62 \text{ dB } \epsilon^{-1}$ , respectively.<sup>[38,151]</sup> In another research, Gu et al. achieved high sensitivity ( $\text{GF} \approx 30$ ) for their optical-type stretchable strain sensor based on the

**Table 1.** Summary of performance results of recently reported polymer-based stretchable strain sensors.

System	Sensor type	Stretchability [%]	Linearity	GF	Response time [ms]	Reference
rGO/TPU	Resistive	100	Two linear regions	11–79	200	[64]
rGO/DI/Ecoflex	Resistive	400	Two linear regions	2.5–31.6	60.3	[65]
Graphene/silicone rubber	Resistive	12	Two linear regions	27.7–164.5	50	[66]
AgNWs/PU fiber/PDMS	Resistive	60	Nonlinear	Up to 9557	120	[121]
Graphene/CNTs/PDMS	Resistive	85	Two linear regions	35	30	[91]
Vertical graphene nanosheets/PDMS	Resistive	110	Linear	32	0.96	[59]
CNTs/CBs/silicone rubber/PDMS	Resistive	120	Linear	1.25	60	[92]
CNFs/GNPs/PDMS	Resistive	50	Linear	Up to 7.04	132	[95]
CNTs/Ecoflex fibers	Resistive	600	Two linear regions	Up to 1378	295	[181]
CNTs nanopaper /PDMS	Resistive	100	Three linear regions	Up to 2.21	50	[105]
Ni NWs/Ecoflex	Resistive	100	Three linear regions	Up to 200	0.32	[119]
PAVG/PDMS	Resistive	10	Linear	5.87–10.28	112	[52]
NiNPs/rGO/PU sponge/PDMS	Resistive	65	Two linear regions	Up to 3360.1	100	[117]
GNPs/CBs/CNTs/PU yarns	Resistive	350	Linear	2.14	65	[172]
CNTs/prestretched PDMS	Resistive	100	Two linear regions	6–87	65	[109]
CNTs/PDMS	Resistive	20	Linear	1140	0.2	[110]
CNTs/PDA/elastic bands	Resistive	920	Four linear regions	5.06–129.2	220	[182]
GWFs/PDMS	Resistive	3	Linear	223	72	[126]
Ti <sub>3</sub> C <sub>2</sub> T <sub>x</sub> /PDMS	Resistive	53	Linear	178.4	130	[10]
CBs/CNTs/silicone rubber	Resistive	50	Linear	2.18	125	[133]
Au NPs/abrasive paper	Resistive	0.59	Linear	Up to 75.8	20	[177]
CNTs/TPU fiber	Resistive	320	Two linear regions	22.1–97.5	200	[137]
CNTs/prestretched TPU	Resistive	300	Three linear regions	428.5–83982.8	70	[138]
Carbon fragments/PDMS	Resistive	80	Two linear regions	2.2–62.8	60	[122]
Aligned rGO/TPU fibers/PDMS	Resistive	150	Linear	593	160	[113]
Ag nanodendrites/ nitrile rubber substrate	Resistive	105	Two linear regions	Up to 294.3	18	[76]
rGO/PDMS	Resistive	350	Three linear regions	18.5–88443	145	[183]
CNTs/Au NPs/prestretched PDMS	Resistive	50	Two linear regions	Up to 70	60	[184]
Parylene/Au film/prestretched elastomeric adhesive	Capacitive	140	Linear	3.05	NA	[15]
Ag NFs/ionic hydrogels	Capacitive	1000	Linear	165	320	[71]
Au NPs/PDMS	Optical	100	Linear	9.54 dB/ε	< 12	[20]
TPU/silicone fiber	Optical	85	Linear	18.75 dB/ε	NA	[28]
PDMS fibers	Optical	100	Linear	3.62 dB/ε	NA	[151]
Polystyrene-based elastomer	Optical	300	Nonlinear	10 dB/ε	NA	[38]
Graphene/PDMS fibers	Optical	100	Linear	13.5 dB/ε	NA	[19]

change of optical transmittance of the CNTs–embedded Ecoflex film.<sup>[42]</sup> They defined the GF as  $\Delta I/I_0\epsilon$ , in which  $\Delta I$  and  $I_0$  are the change in the light intensity and the initial light intensity, respectively.

### 6.3. Linearity

The linearity of a strain sensor is quantified by the coefficient of determination ( $R^2$ ) obtained from a linear regression. A linear strain sensor has a larger  $R^2$  value with a negligible deviation of the output signal from a straight line. In contrast, a strain

sensor is considered to be nonlinear if  $R^2$  is small.<sup>[1,11]</sup> The linear response of stretchable strain sensors over a large strain range is highly desirable as the nonlinearity adds complexity to the calibration and data processing of the output signal.<sup>[1]</sup> Overall, the linearity of capacitive and optical strain sensors is greater than that of resistive-type strain sensors (Table 1 and 2). The nonlinear response of resistive-type strain sensors is attributed to the non-homogeneous microstructural and morphological changes in the sensing films upon stretching.<sup>[1]</sup> CNT polymer nanocomposite-based strain sensors have typically exhibited nonlinear electro-mechanical response.<sup>[54,69,102,123]</sup> The majority of recently

**Table 2.** Summary of performance results of recently reported resistive-type textile strain sensors.

System	Stretchability [%]	Linearity	GF	Response time [ms]	Reference
Carbonized silk fabric/Ecoflex	500	Two linear regions	9.6–37.5	70	[149]
rGO/cotton bandage	57	Two linear regions	416–3667	20	[163]
GNPs/CBs/fragmented cotton fabric/Ecoflex	400	Three linear regions	95.64–102351	97	[145]
GNPs/CBs/flax yarn/Ecoflex	12.5	Linear	Up to 5.62	209	[144]
GNPs/CBs/wool yarn/Ecoflex	200	Two linear regions	5.05–7.75	172	[143]
Carbonized silk georgette/PDMS	100	Two linear regions	29.7–173	70	[152]
GNPs/CBs/wool fabric/Ecoflex	150	Two linear regions	Up to 0.5	NA	[146]
GNPs/CBs/cotton fabric/Ecoflex	150	Two linear regions	1.67–6.05	NA	[146]
Carbonized cotton/Ecoflex	140	Two linear regions	25–64	NA	[148]

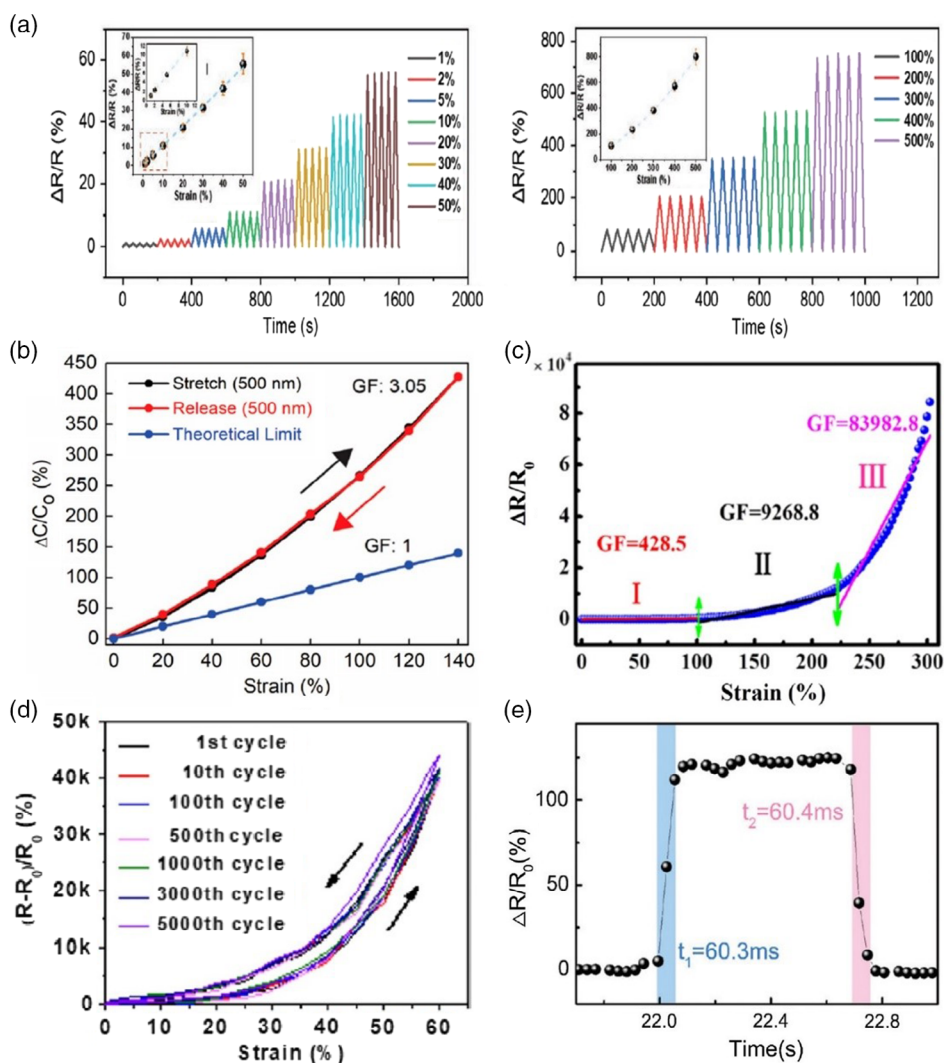


**Figure 7.** Electromechanical performance of various polymer-based stretchable strain sensors. a) Cyclic stretching-releasing of the sandwiched graphene/PAA/ACC-based strain sensor, showing its ability to measure both small and large strains. Reproduced with permission.<sup>[141]</sup> Copyright 2019, Wiley-VCH. b) Capacitive response of the wrinkled Au-film electrodes-based strain sensor during loading and unloading cycles with high GF and linearity. Reproduced with permission.<sup>[15]</sup> Copyright 2018, American Chemical Society. c) Relative resistance changes of the cracked-based CNTs-TPU strain sensor with high sensitivity and linear response in three strain ranges. Reproduced with permission.<sup>[138]</sup> Copyright 2019, American Chemical Society. d) Hysteresis loops of a  $Ti_3C_2T_x$ -AgNW-poly(dopamine)/ $Ni^{2+}$  strain sensor subjected to 5000 stretching and releasing cycles. Reproduced with permission.<sup>[80]</sup> Copyright 2019, American Chemical Society. e) Response and recovery time of the rGO/DI strain sensor, indicating its fast response and recovery to external loads. Reproduced with permission.<sup>[65]</sup> Copyright 2018, Royal Society of Chemistry.

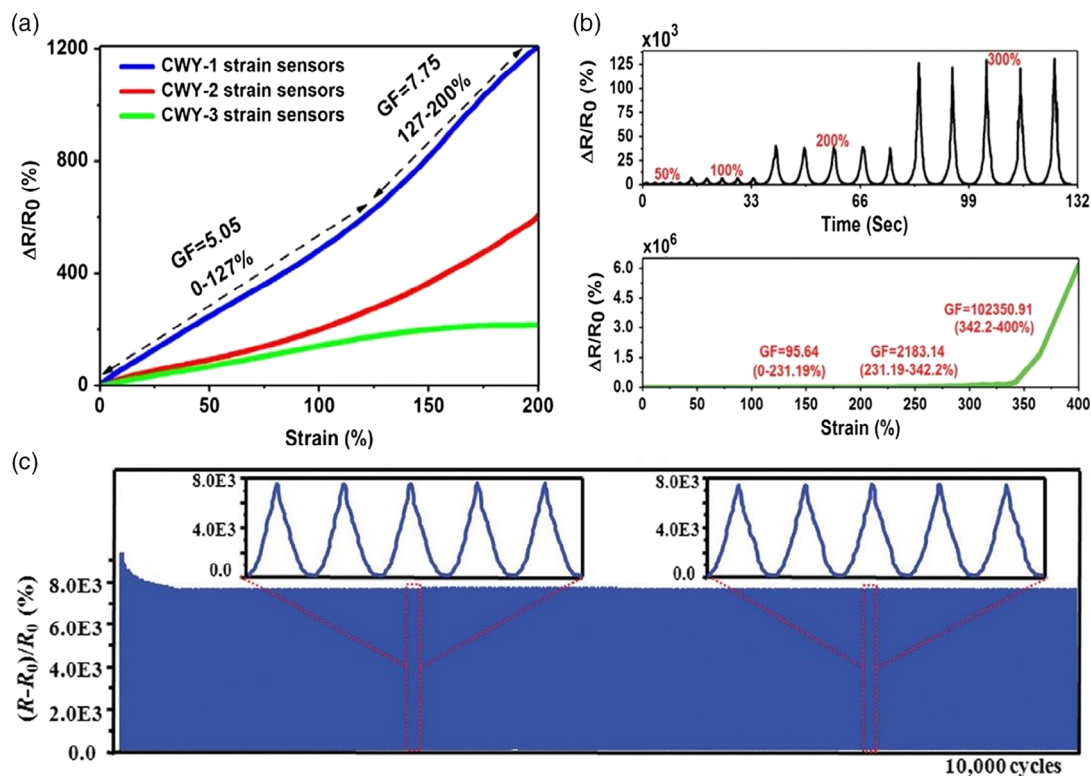


**Figure 8.** Electromechanical performance of conductive natural fiber-based stretchable strain sensors. a) Controlling the sensitivity of strain sensors based on conductive wool yarns–Ecoflex composite by geometric engineering. Reproduced with permission.<sup>[143]</sup> Copyright 2019, Elsevier. b) Electromechanical performance of the fragmented conductive cotton fabric–Ecoflex composite strain sensor. Reproduced with permission.<sup>[145]</sup> Copyright 2018, Royal Society of Chemistry. c) Durability of the carbonized silk georgette-based strain sensor to 10 000 stretch-release cycles. Reproduced with permission.<sup>[152]</sup> Copyright 2017, Royal Society of Chemistry.

reported resistive-type strain sensors have shown linear response in two or three regions (Table 1 and 2).<sup>[90,91,97,145,149]</sup> For instance, a self-healing and highly stretchable ionogel-based strain sensor illustrated electromechanical response in two linear regions (0–800% and 800–1400%) in its entire working strain range.<sup>[90]</sup> In another study, a highly stretchable strain sensor based on the fragmented conductive cotton fabric responded to the applied strain in three linear regions (0–231%, 231–342%, and 342–400%) (Figure 7c).<sup>[138]</sup> Some of the stretchable strain sensors have also shown excellent linearity. Shintake et al.,<sup>[53]</sup> Nur et al.,<sup>[15]</sup> Atalay et al.,<sup>[164]</sup> Xu et al.,<sup>[71]</sup> and Ling et al.<sup>[186]</sup> reported capacitive-type strain sensors that are linear up to 500%, 140%, 80%, 1000%, and 100% strains, respectively.

The response of stretchable optical strain sensors is typically highly linear. Optical strain sensors based on the PDMS elastomer showed high linearity up to the tested range (0–100%) of tensile strain.<sup>[151]</sup> In another study, a TPU/silicone stretchable optical waveguide showed high linearity up to 85% of tensile strain.<sup>[28]</sup> Although most of the optical strain sensors show a linear response, a nonlinear response was also observed for a highly stretchable optical strain sensor made of a polystyrene-based core and a fluorinated polymer cladding.<sup>[38]</sup>

On an overall basis, the development of strain sensors with highly stretchable, sensitive, and linear electromechanical response is still a grand challenge. A trade-off relationship between “high stretchability and linearity” and “high sensitivity”

has often been observed in the majority of stretchable strain sensors (Table 1 and 2). Highly sensitive strain sensors typically show high nonlinearity (or linearity in multiple regions) and limited stretchability, and vice versa. For example, stretchable strain sensors based on the formation of microcracks and disconnection mechanism have exhibited higher sensitivities compared with those with other sensing mechanisms, but with high nonlinearity.

#### 6.4. Hysteresis

Hysteresis of a strain sensor is defined as the dependency of its current state (i.e., output signal of cycle  $n$ ) on its history (i.e., output signal of cycles 1 to  $n - 1$ ) (Figure 7d). Hysteresis is an important factor of any strain sensor, especially in wearable applications where strain sensors are frequently subjected to dynamic loading conditions.<sup>[23]</sup> High hysteresis behavior leads to the nonmonotonic response of a strain sensor under cyclic loading.<sup>[1,11,23]</sup> Overall, capacitive-type strain sensors show less hysteresis than resistive and optical strain sensors.<sup>[1,23,37]</sup> This could be explained by the fact that the performance of capacitive-type strain sensors relies on the stable overlapped area between the pair of electrodes.<sup>[1]</sup> In stretchable resistive strain sensors, the viscoelastic nature of the polymeric substrates, as well as their interaction with active nanomaterials contribute

to the hysteresis behavior. In addition, the reconnection of nanomaterials (e.g., ohmic or tunneling contact) during the release cycle takes time and can be even irreversible though they return to the original positions. As a result, strong interfacial bonding between the active sensing nanomaterial and substrate or matrix minimizes the hysteresis.<sup>[23,37,143,145]</sup> Conversely, weak binding retards the fast recovery of nanomaterials to their initial positions during the releasing cycle, leading to a high hysteresis effect. The CNTs-based strain sensors have been reported to have higher hysteresis behavior compared with other nanomaterials, mainly due to the weak interfacial bonding between CNTs and polymers.<sup>[1,11,23]</sup> In contrast, very strong interfacial binding could result in buckling and fracture of nanomaterials. Therefore, an optimal interfacial adhesion between rigid nanomaterials and stretchable substrate/matrix materials gives the best hysteresis performance in resistive-type strain sensors.

The stretchable optical strain sensors have also exhibited negligible hysteresis compared to resistive-type strain sensors. For instance, strain sensors made of TPU/silicone and PDMS fibers responded to dynamic strains with almost no hysteresis effect.<sup>[28,151]</sup> In contrast, a thermoplastic elastomer-based optical strain sensor showed little hysteresis in cyclic strain.<sup>[38]</sup> Overall, the negligible hysteresis in the response of capacitive and optical stretchable strain sensors can be attributed to the fact that their response does not rely on the formation of ohmic contact or tunneling conduction between nanomaterials, which can often be irreversible over repeated stretching–releasing cycles.

### 6.5. Response and Recovery Time

The response time of a strain sensor is expressed as the amount of time needed for the sensor to reach a steady-state response. This time could be delayed due to the viscoelastic behavior of elastomers, as one of the key elements of stretchable strain sensors.<sup>[1]</sup> Response time can be either directly measured from the experiment (Figure 7e) or theoretically calculated through 90% time constant.<sup>[8,23,143,145]</sup> Stretchable strain sensors have illustrated diverse response times ranging from 0.2 to 320 ms (Table 1 and 2). PDMS-based resistive strain sensors showed faster response time compared with those made of the Ecoflex elastomer, mainly due to the ultrasoftness of Ecoflex providing lower recovery force for the rapid reformation of conductive percolative networks of active nanomaterials during the releasing cycle.<sup>[9]</sup> Natural fiber-based stretchable strain sensors have shown short response time, making them an ideal alternative for wearable applications (Table 2).<sup>[143–145,148]</sup> Another crucial performance parameter of a stretchable strain sensor, especially under cyclic loads, is recovery time, which could be in the order of sub-seconds to a few seconds.<sup>[37,40,41]</sup> Generally, stretchable strain sensors based on nanocomposites have shown longer recovery time largely because of the existence of friction between conductive fillers and polymer matrices. This friction force delays the recovery of conductive networks in the releasing cycle.<sup>[1,41]</sup>

### 6.6. Overshoot Behavior

Overshooting in the output signal of sensors has been reported in many stretchable strain sensors.<sup>[1]</sup> The main reason for such

a behavior is the stress relaxation of polymeric substrates or matrices. Wearable resistive-type strain sensors have typically demonstrated larger overshoot compared with capacitive and optical sensors. This is due to the instant stress release of polymeric substrates or matrices when strain sensors are subjected to a suddenly applied strain.<sup>[1,23,37]</sup> The internal structure of polymers and their movement under external load also contribute to overshooting behavior. In the case of capacitive-type strain sensors, these movements have minimum effect on the permittivity of the dielectric layer; hence small overshooting occurs in their response. In contrast, the internal structure movements can alter the location of conductive nanomaterials, directly affecting the overall resistance of strain sensors.<sup>[1]</sup> Therefore, the overshooting is more pronounced in the resistive-type strain sensors. In addition to the aforementioned parameters, strain rate and viscoelasticity of polymers influence the overshooting behavior of strain sensors. We believe that overshooting can be minimized by tuning the molecular or molecular segment motions of polymeric substrates under large strains.<sup>[1]</sup> In addition, the optimized interaction between active materials and substrates is necessary so that the stress relaxation of the substrate would have less effect on the structural movement of the active materials.<sup>[1]</sup>

### 6.7. Dynamic Durability

The endurance of a strain sensor to long-term stretching–releasing cycles is a crucial factor that is known as dynamic durability. A durable strain sensor possesses stable response and mechanical integrity during long-term cyclic loads. Durable strain sensors are ideal for wearable strain sensing applications where large and dynamic strains should be accommodated by them. Highly durable and stretchable strain sensors have been recently reported in which they have shown remarkable dynamic durability up to 20 000 stretching–releasing cycles<sup>[62,64,111,112,122,138,139,177,182,187,188]</sup> even at very high strain levels (150%).<sup>[72]</sup> Wang et al. stepped even beyond this limit and developed a strain sensor based on CNTs/cotton/TPU core–spun yarn that was durable up to 300 000 cycles at 40% strain.<sup>[189]</sup> The high durability of the strain sensor could be due to the highly elastic behavior of CNTs, avoiding their plastic deformation and fracture under dynamic loading. As an example of natural fiber-based strain sensors, a sensor based on the carbonized silk georgette fabric encapsulated with PDMS showed excellent dynamic durability up to 10 000 stretching–releasing cycles (Figure 8c).<sup>[152]</sup>

## 7. Applications of Stretchable Strain Sensors

There are several applications for stretchable strain sensors ranging from the detection of various human body movements (respiration, heartbeat, body joints, etc.) to human–machine interaction, interactive gaming, and virtual reality.

### 7.1. Healthcare and Biomedical Engineering

Stretchable strain sensors are important healthcare monitoring devices because they continuously capture a wide range of body motions from large joint movements to subtle deformations

originated from physiological signals (e.g., pulse or respiration rates). To monitor the low strains, highly sensitive sensors are needed to give high resolution and accurate signal variations in response to tiny deformations.<sup>[178]</sup> **Figure 9a** shows a stretchable strain sensor attached to the radial artery of the wrist for pulse rate monitoring.<sup>[56]</sup> The resistance of the sensor increased in each cardiac cycle due to the minute strains induced by the blood flow pressure. Furthermore, the sensor was able to sufficiently identify the pulse features, such as percussion, tidal, and diastolic waves. **Figure 9b** shows an e-skin apexcardiogram (ACG) strain sensor for tracking the temporal volume and pressure changes in the heart.<sup>[79]</sup> The metal NPs–elastomer composite sensor was attached to the apex region in the fifth intercostal space, and its response was measured in real time. **Figure 9c** shows the recorded ACG waveform for a healthy volunteer, revealing accurate detection of hemodynamic parameters, such as the opening and closing events of the atrioventricular valve (points “O” and “C”), rapid ventricular filling wave (O–F region), slow ventricular filling wave (F–L region), ventricular filling (peak “A”), ventricular contraction (peak “E”), and end-systolic shoulder (ESS). These results were further validated by

conventional electrocardiogram (ECG) signals. **Figure 9d,e** show the comparison of the ACG signals of the volunteer recorded in the rest mode and after exercise. Notably, the sensor could simultaneously capture respiration rate and ACG. The respiration rate was increased from 12 min<sup>-1</sup> before exercise to 26 min<sup>-1</sup> after exercise. As shown in figures, the signal amplitude of the sensor greatly enhanced during the exercise, showing larger strains accommodated by the sensor due to the deep breathing. In contrast, the period of the cardiac cycle decreased from 0.85 to 0.54 s after exercise. Continuous monitoring of the heart performance and respiration by means of wearable strain sensors can, therefore, provide useful medical information for the early diagnosis of various diseases, including asthma, anemia, heart failure, and embolism.<sup>[6,79,190]</sup>

Stretchable strain sensors have also been utilized for the phonetic recognition and detection of emotional expression.<sup>[10,33,56,71,148]</sup> To monitor the phonetics, a carbonized cotton fabric-based stretchable strain sensor was attached to the throat of a volunteer to detect the tiny muscle movements during speaking (**Figure 9f**).<sup>[148]</sup> When the wearer pronounced different words (“Cotton,” “Sensor,” and “Hello”), the strain sensor produced

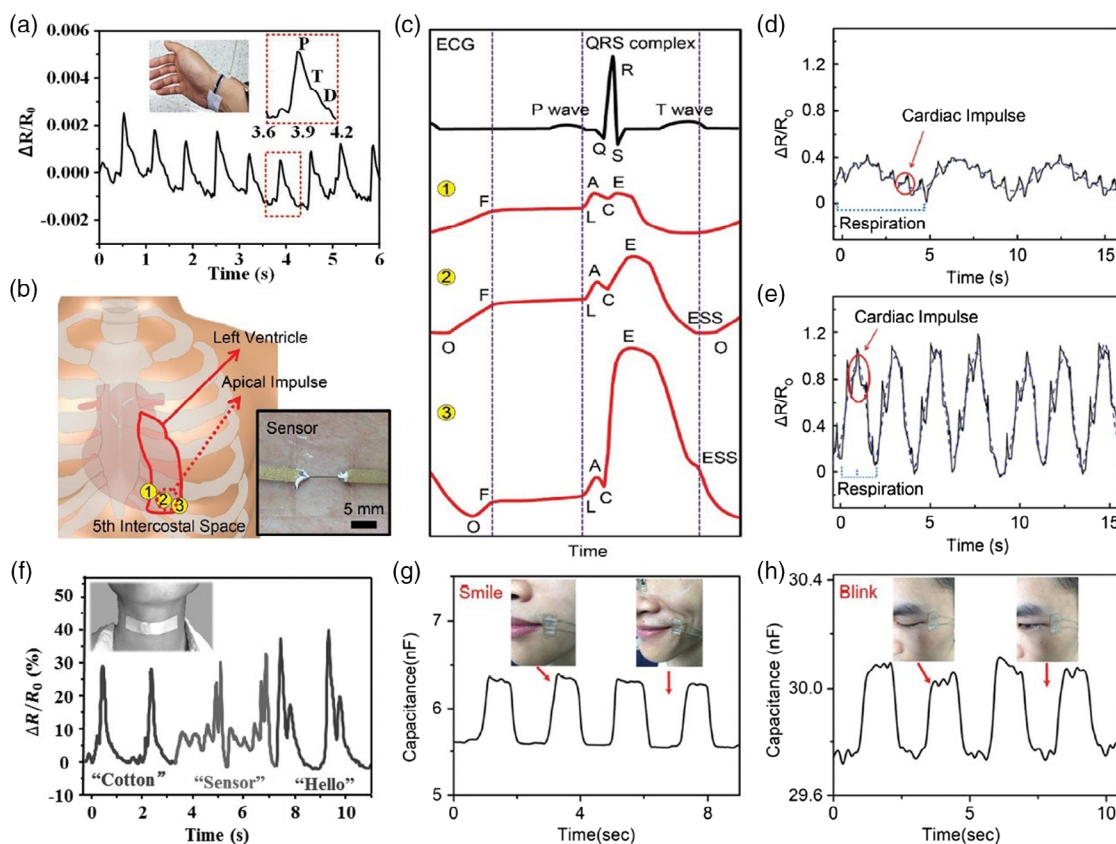


**Figure 9.** Low-strain applications of stretchable and highly sensitive strain sensors. a) The resistance change of a stretchable strain sensor with respect to the blood flow pressure in the wrist. Reproduced with permission.<sup>[56]</sup> Copyright 2019, Wiley-VCH. b) Schematic illustration of the locations of the mounted ACG sensor and photograph of the metal NPs–PDMS composite ACG strain sensor. c) Response of the sensor at different locations and its comparison with the ECG signal. d) Response of the ACG sensor of the volunteer in the rest state. e) Response of the ACG sensor after exercise. b–e) Reproduced with permission.<sup>[79]</sup> Copyright 2016, Wiley-VCH. f) Output signal of a carbonized cotton fabric-based stretchable strain sensor placed onto the throat during the speaking. Reproduced with permission.<sup>[148]</sup> Copyright 2016, Wiley-VCH. g) Capacitive-response of the Ag NFs-ionic hydrogel nanocomposite strain sensor attached to the mouth during smiling action. h) Response of the Ag NFs-ionic hydrogel nanocomposite strain sensor to the eye closing–opening movements. g,h) Reproduced with permission.<sup>[71]</sup> Copyright 2019, Royal Society of Chemistry.



repeatable and distinguishable signals for each word with unique amplitude and waveform. The phonation recognition using wearable strain sensors is beneficial in human-machine interaction and phonation rehabilitation.<sup>[33]</sup> Figure 9g,h show the capability of wearable strain sensors in identifying facial and emotional expressions. A stretchable capacitive-type strain sensor was mounted around the mouth and corner of the eye, and its capacitive-response was measured during smiling and eye closing-opening movements, respectively.<sup>[71]</sup> As shown in the figures, the strain sensor detected both actions with high sensitivity and reversible response. Monitoring of psychological distress through human emotions such as smiling and wrinkling is a useful tool for the assessment of diseases like Alzheimer's disease.<sup>[71]</sup>

For large-strain human motion detection, stretchable strain sensors have been attached to finger, wrist, elbow, and knee joints to track the body activities.<sup>[9,33,56]</sup> Figure 10a shows an overlapped CNT stretchable strain sensor fixed to the joints of the index finger and its corresponding output signal during repeated bending-straightening of the finger.<sup>[56]</sup> The resistance of the sensor increased when the bending angle increased in a stepwise manner. A similar electromechanical response was observed when the sensor was mounted onto the elbow joint (Figure 10b). The strain sensor successfully measured the accommodated strain under the fully bent elbow, corresponding to strains as large as 60%.<sup>[9,56]</sup> Figure 10c shows the resistive

response of a graphene fiber stretchable strain sensor placed onto the knee.<sup>[2]</sup> The sensor differentiated various knee-related movements, including flexing-extending, walking, jogging, jumping, and squatting-jumping. These results could be beneficial in biomechanics, physiology, and kinesiology applications.<sup>[8]</sup>

## 7.2. Sport Performance Monitoring

Wearable strain sensors offer new integrated platforms for assessing the biomechanical and physiological parameters of athletes.<sup>[191,192]</sup> Stretchable strain sensors can intimately couple with different locations of the body, resulting in highly localized tracking of sport activities.<sup>[1,192]</sup> Real-time monitoring of biophysical parameters such as respiration and heart rates through wearable strain sensors provides deep insights into the physiological health state of athletes before, during, and after physical activities (Figure 9). Figure 11a shows the use of wearable graphene-fiber strain sensors for monitoring the gesture of a soccer player during the shooting event.<sup>[192]</sup> The strain sensors were attached to the knee, ankle, and elbow of the player, and their sensory response was recorded. As shown in the figure, the strain sensors were able to monitor the entire process of soccer shots, providing detailed data for the analysis of the shooting gesture. In another example, wearable strain sensors were attached to the knee, and the gesture of squatting and leg lifting was successfully monitored (Figure 11b,c).<sup>[191]</sup> These results suggest that wearable

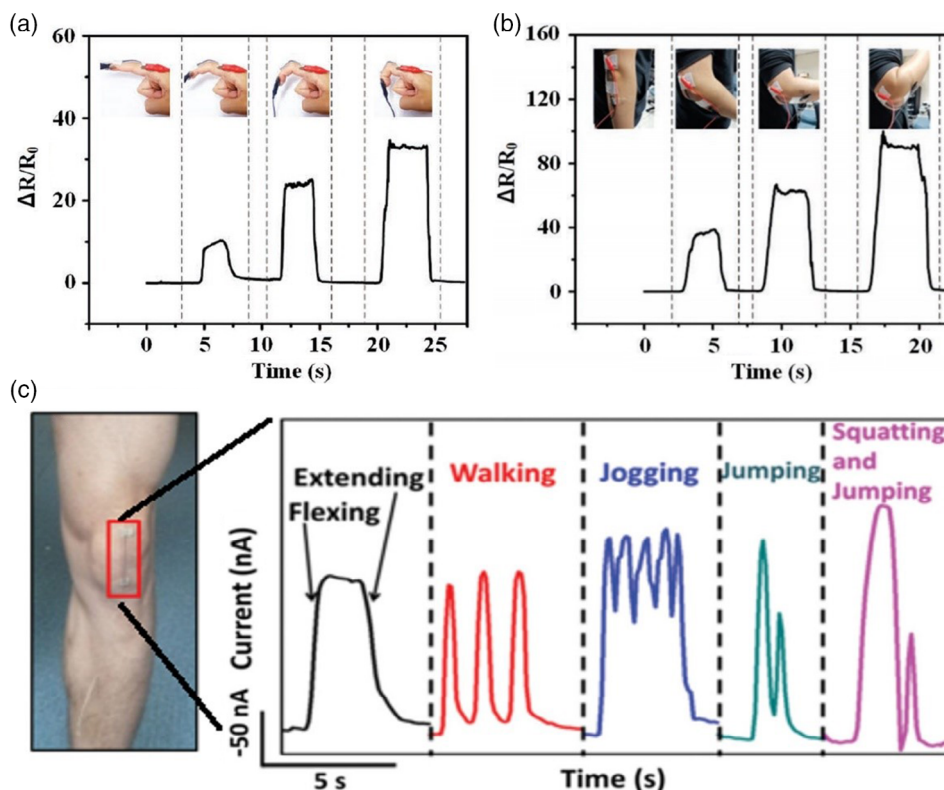


**Figure 10.** Applications of stretchable strain sensors in the large-strain motion detection. a) Response of a stretchable strain sensor to the finger bending motions. b) Resistance change of a strain sensor under elbow bending movements. a,b) Reproduced with permission.<sup>[56]</sup> Copyright 2019, Wiley-VCH. c) Photograph and response of a graphene fiber strain sensor attached to the knee under flexing/extending, walking, jogging, jumping, and squatting-jumping. Reproduced with permission.<sup>[2]</sup> Copyright 2015, Wiley-VCH.

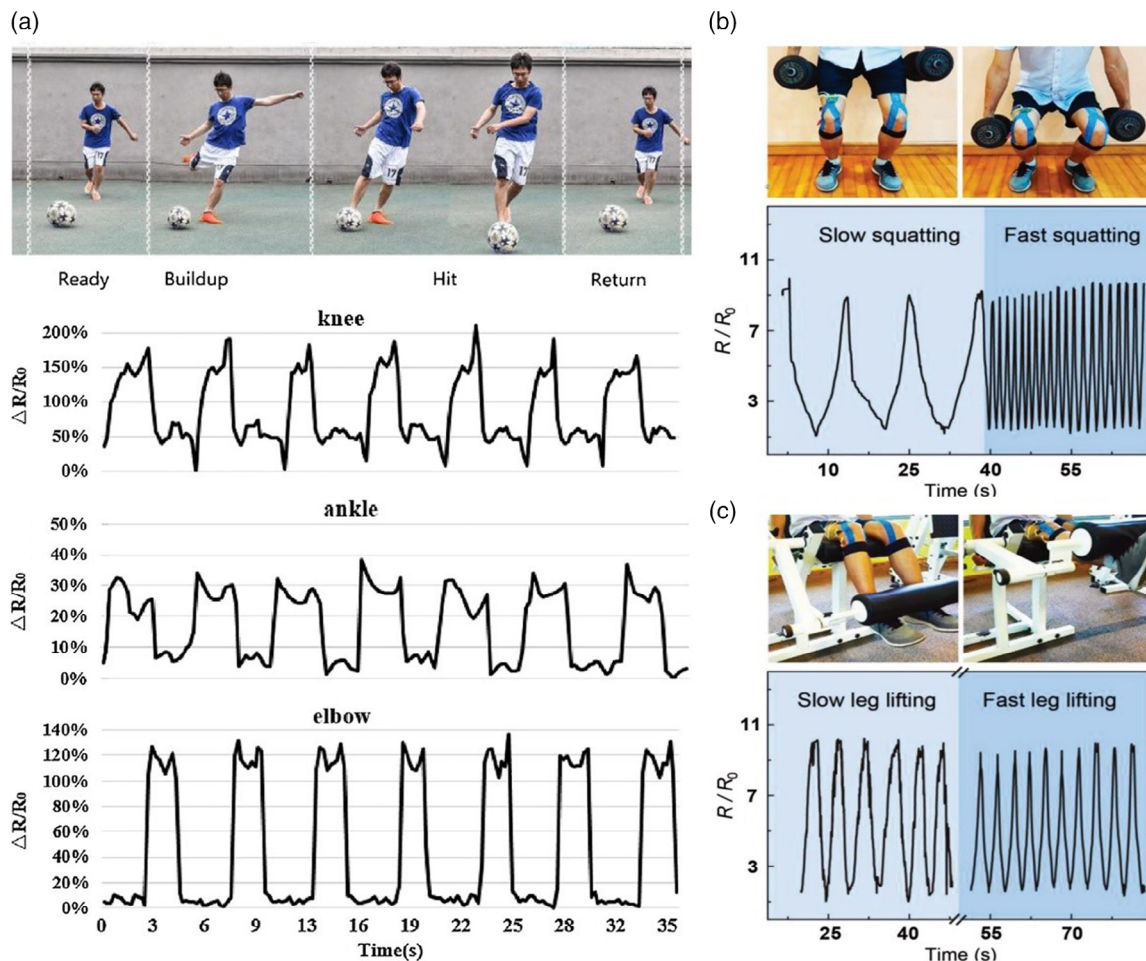


**Figure 11.** Wearable strain sensors for the analysis of sport performance. a) Photographs of a soccer play during the shooting event and corresponding response of strain sensors attached to the knee, ankle, and elbow. Reproduced with permission.<sup>[192]</sup> Copyright 2018, Elsevier. b) Response of a stretchable strain sensor attached to the knee during squatting movements. c) Response of a stretchable strain sensor attached to the knee during leg lifting. b,c) Reproduced with permission.<sup>[191]</sup> Copyright 2017, Wiley-VCH.

and stretchable strain sensors are desirable for the continuous monitoring of health and wellness conditions, human-friendly rehabilitation, and evaluation of athletes' sport performance.<sup>[1]</sup>

### 7.3. Interactive Gaming and Virtual Reality

As another potential application, wearable strain sensors can serve as motion sensors for entertainment technology and virtual reality.<sup>[1,8,32,36,193]</sup> Figure 12a shows an example of the interactive gaming using stretchable strain sensors. Graphene strain sensors were attached to the hand fingers, and their resistance changes upon bending–straightening of the fingers were used as commands to play a video game.<sup>[193]</sup> As body movements are needed for posture-driven gaming, wearable sensors may find applications in medical training, home-rehabilitation, and physiotherapy.<sup>[1,194]</sup> Figure 12b shows an integrated smart glove system made of wearable optical fiber-based strain sensors placed in each finger for capturing the hand movements.<sup>[38]</sup> The finger positioning data were used to control a virtual

3D hand model in real time. In another work, Amjadi et al. developed a fully integrated smart glove composed of the Ag NWs-PDMS nanocomposite-based wearable sensors and a miniaturized multifunctional electronic chip, and demonstrated successful control of an avatar in the virtual environment.<sup>[8]</sup> Thus, wearable strain sensors could be used to intuitively interact with the virtual environment or to control internet-of-things devices and teleoperated robotic systems.<sup>[1,6,8,38]</sup>

### 7.4. Soft Robotics and Neuromechanics

Emerging technologies in stretchable strain sensors are increasingly enabling novel proprioceptive interactions with unstructured environments. For instance, a fully functional soft prosthetic hand with integrated stretchable optoelectronic strain sensors has been developed to effectively differentiate ripe tomatoes from unripe ones.<sup>[28]</sup> Qu et al. attached super-elastic fiber strain sensors to soft robotic fingers for haptic perception.<sup>[166]</sup> Larson et al. reported a hyperelastic light-emitting

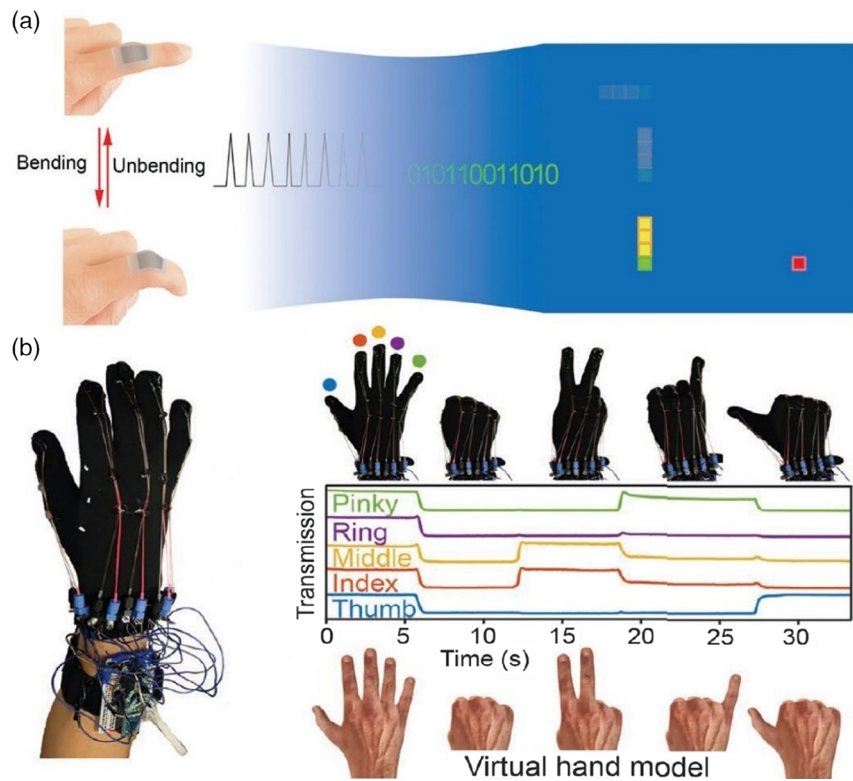


**Figure 12.** Application of stretchable strain sensors in gaming and virtual reality. a) Interactive gaming using a graphene-based stretchable sensor. Reproduced with permission.<sup>[193]</sup> Copyright 2018, Wiley-VCH. b) An integrated smart glove system featuring optical fiber-based strain sensors in each finger for the control of a virtual hand model. Reproduced with permission.<sup>[38]</sup> Copyright 2018, Wiley-VCH.

capacitor (HLEC)-based tactile sensing platform that can change illuminance and capacitance under deformation (Figure 13a).<sup>[195]</sup> HLEC skin was embedded into a soft crawling robot that changes the capacitance (up to 1000%) upon pneumatic actuation. Even though pneumatic actuation is heavily utilized in the field of soft robotics, the use of sensory feedback is still in its nascent stage.<sup>[197–199]</sup> To improve the combination of pneumatic actuators with stretchable strain sensors, a sensorized actuated glove has been developed to perform accurate finger kinematics with dexterity and control for rehabilitation applications.<sup>[200]</sup> In a similar study, Cheng et al. demonstrated a pneumatic actuator with the capability of the bending angle monitoring using a hydrogel-based stretchable strain sensor (Figure 13b).<sup>[196]</sup> Stretchable microcracks-based strain sensors have been integrated with a two-finger soft robotic gripper for activity monitoring (Figure 13c).<sup>[6]</sup> It has been shown that the touch status, contact force, and bending position of the soft gripper finger could be tracked via the intertwined strain sensors. In another study, Truby et al. 3D-printed ionically conductive gels with the soft somatosensitive actuators (SSAs) for strain sensing (Figure 13d).<sup>[29]</sup> They demonstrated the combination of the sensor and actuators in haptic and proprioceptive sensing applications.

Soft and stretchable strain sensors could play a major role in the study of morphological intelligence. Applications include smart rehabilitative devices, gesture recognition based on haptic feedback, soft robotic grippers, and in building artificial electronic skin (e-skin).<sup>[29,30,78,201–207]</sup> For example, Guo et al. built a

stretchable optical strain sensor that can further be used for soft rehabilitative gloves and biomechanics research for ultrasensitive physiological activities.<sup>[20]</sup> Similarly, in minimally invasive surgery, there is a great demand to combine biocompatible soft sensors with surgical instruments for better navigation and control.<sup>[208]</sup> In this regard, Banerjee et al. demonstrated successful cadaver trials that incorporate soft sensing for effective drug delivery, as well as variable stiffness modulation based on origami engineering.<sup>[209,210]</sup>

Wearable and skin-mountable sensors could be helpful in robophysical models to provide insight in the neuromechanics of locomotion.<sup>[211–214]</sup> Neuromechanics pertains to multiple physiological systems interacting to generate behavior in living organisms (Figure 14a). Attempting to decipher the neuromechanics of the locomotion involves the capturing of neuronal activity, the dynamics of the musculo-skeletal system, as well as the interaction of the body with the external environment. To gain insight in the underlying processes of reflexes and passive dynamics, one can integrate stretchable strain sensors for sensory feedback (Figure 14b). For example, a liquid metal-based hyperelastic strain sensor has shown a great promise to effectively measure the human gait.<sup>[218]</sup> In a recent study, Kim et al. demonstrated a similar soft exosuit that promised to reduce metabolic rates while a person is subjected to motion vis-à-vis running.<sup>[219]</sup>

Robots are increasingly envisaged to enter into tasks that involve contact with humans. To make a safer human–machine interaction, it is needed to redesign robots that mimic soft natural organisms (Figure 14c). In this regard, animal locomotion

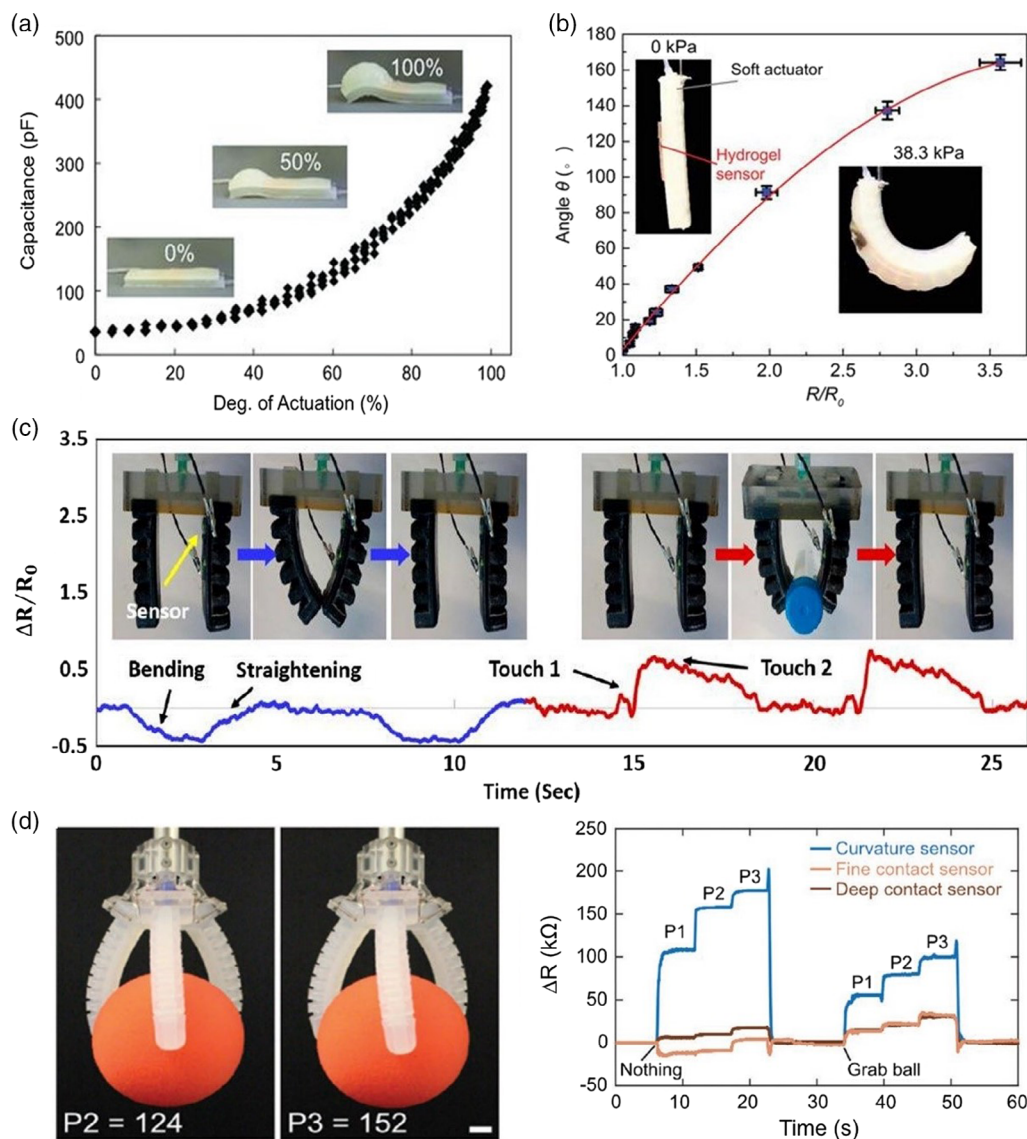


**Figure 13.** Applications of strain sensors in soft robotics. a) HLEC-based strain sensor for monitoring the degree of the pneumatic actuation in a soft robotic crawler. Reproduced with permission.<sup>[195]</sup> Copyright 2016, American Association for the Advancement of Science. b) A pneumatic actuator bending angle monitoring with a hydrogel-based stretchable strain sensor. Reproduced with permission.<sup>[196]</sup> Copyright 2019, Wiley-VCH. c) Microcracks-based strain sensors integrated into a soft robotic gripper. Reproduced with permission.<sup>[6]</sup> Copyright 2016, American Chemical Society. d) A soft gripper composed of SSAs with embedded curvature, and fine and deep contact sensors. Reproduced with permission.<sup>[29]</sup> Copyright 2018, Wiley-VCH.

provides great fundamental motivation for roboticists to design softer robots.<sup>[220]</sup> For instance, the neuromechanics of axial muscle cocontraction during undulatory swimming can be effectively modeled using pairs of soft actuators, yielding discovery of maximum thrust via body stiffness modulation by Jusufi et al.,<sup>[216]</sup> thus, facilitating exploration of a wider parameter space than live animal experimentation alone.<sup>[216,221]</sup> Moreover Wright et al. integrated a soft strain sensor with a soft actuator to monitor the undulation of a soft robotic fish (Figure 14d).<sup>[167]</sup> These findings demonstrate an immediate need to integrate stretchable strain sensors as a closed-loop solution for the body caudal-fin swimming that can improve maneuverability of biologically inspired robots (Figure 14e).<sup>[222–226]</sup> These novel soft

active materials based sensing solutions, once integrated, will result in the design and manufacturing of more life-like machines.

Roboticists are increasingly cooperating with biologists to study mechanisms via soft robotic physical models with more animal like capabilities.<sup>[214]</sup> These physical models can provide a tool for biologists to test a larger parameter space than would be possible with live animal experimentation, and thus assist in hypothesis testing of locomotion dynamics, swimming behavior, and how the muscle and skeletal systems adapt functionalities in complex environments (e.g., in sand, soils, and land). In this context, stretchable strain sensors have potential to provide reliable sensory feedback that can yield robust capabilities. The modeling of animal locomotion while moving in a granular

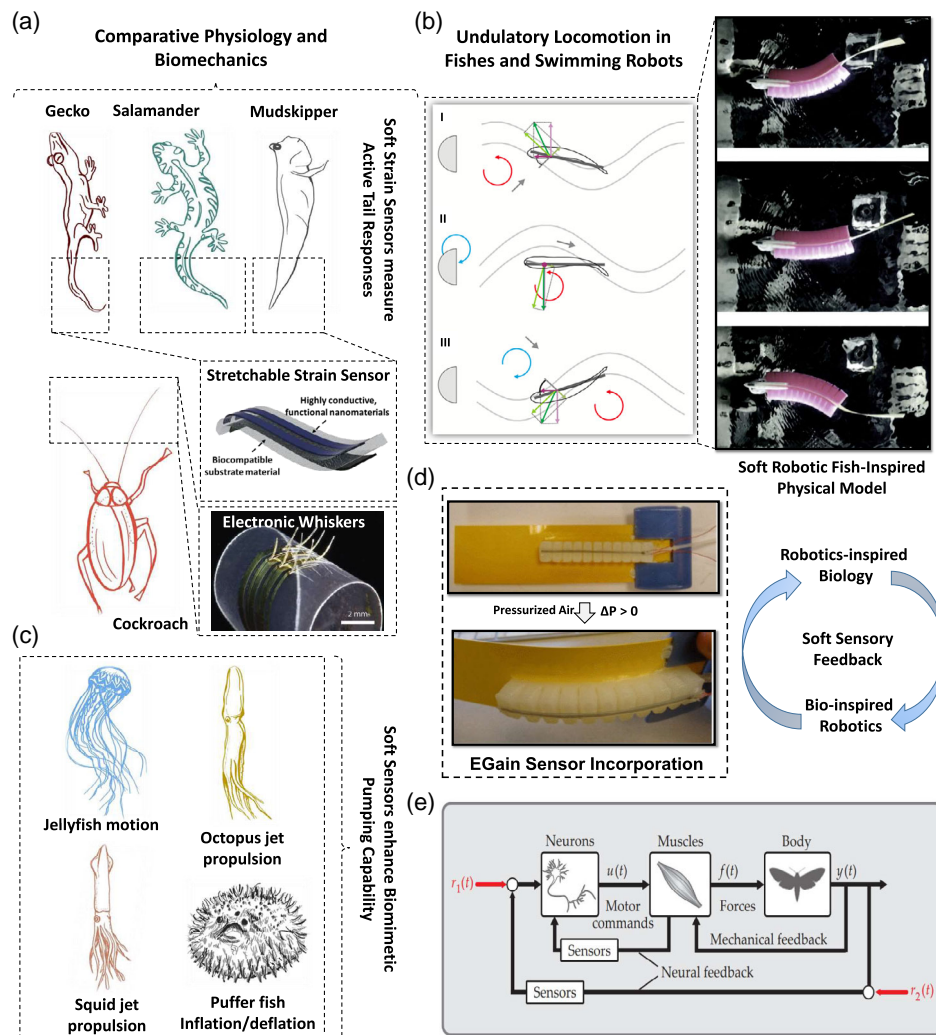


**Figure 14.** Applications of soft strain sensors in locomotion, biorobotics, and neuromechanics. a) Soft and stretchable strain sensors for comparative physiology and biomechanics study (electronic whiskers). Reproduced with permission.<sup>[215]</sup> Copyright 2018, Wiley-VCH. b) Study of fish fin mimicking undulation swimming and midline kinematics with the aid of soft robotics fish-inspired physical model. Left panel (I, II, and III): Reproduced with permission.<sup>[217]</sup> Copyright 2003, Company of Biologists LTD. Right panel (Soft Robotic Fish-Inspired Physical Model): Reproduced with permission.<sup>[216]</sup> Copyright 2017, Mary Ann Liebert, Inc. c) Stretchable strain sensors enhance biomimetic pumping systems that model aquatic organisms. d) Hyperelastic soft sensors enable curvature estimation of body caudal fin swimming in a soft robotic fish. Reproduced with permission.<sup>[167]</sup> Copyright 2019, IEEE. e) Animal movement represented by a neuromechanical system diagram. Soft sensory feedback bridges the gap between robotics-inspired biology with the bioinspired robotics. Reproduced with permission.<sup>[213]</sup> Copyright 2017, American Institute of Physics.

medium, stretchable sensors can be intertwined with the robot body that can provide information about slip and average inclination.<sup>[220]</sup> In the process of developing more life-like robustness, soft strain sensors can be utilized to test model systems of locomotion in nature (e.g., gecko, cockroach, mudskipper, and salamander) to reveal striking fundamentals (Figure 14a,d).<sup>[216,221,227]</sup> Beyond comparative biomechanics research, applications of stretchable sensors could potentially extend to include diagnostics in veterinary care.

## 8. Limitations and Challenges

With recent advances in materials science and functional microstructures/nanomaterials, wearable strain sensors have

demonstrated promising sensing performance for the potential applications in human motion detection and soft robotics. However, several challenges associated with the design, integration, and safety of wearable and stretchable strain sensors still exist. Herein, we address some of the major challenges in the design of high-performance wearable strain sensors for their practical implementation.

First, the development of stretchable strain sensors capable of measuring decoupled strains in multidirections and multiplane deformations is still challenging.<sup>[1,78]</sup> Further research activities should be directed to novel sensing architecture, 3D structures, and metamaterials to overcome this limitation.<sup>[228]</sup> Despite the intense research in the design of wearable strain sensors offering both high stretchability and sensitivity in recent years, the

majority of the current stretchable strain sensors suffer from nonlinear response and hysteresis behavior, making calibration process complicated for high-strain applications like human motion detection where large and dynamic strains are subjected strain sensors.<sup>[1]</sup> In addition, the output signal of many reported strain sensors is vulnerable to pressure as well as variations in environmental conditions such as changes in temperature and humidity. A recent study revealed a significant influence of temperature and humidity changes on the strain sensing behavior of CNTs–PDMS nanocomposite strain sensors.<sup>[229]</sup> Thus, new material approaches, advance packaging strategies, and micro-/nanostructure designs are required to eliminate these unwanted interferences.<sup>[197,230,231]</sup> For example, a temperature self-compensated hybrid film composed of graphite and CNTs has been proposed to decouple the effect of the temperature change on the response of strain sensors.<sup>[197]</sup> Super-hydrophobic coatings have been utilized to prevent the penetration of water molecules into the strain sensing films.<sup>[230,232]</sup> Zhang et al. have reported that sandwiching CNTs–Ecoflex nanocomposite strain sensors between two layers of Ecoflex can greatly enhance their endurance to humidity variations.<sup>[233]</sup>

Second, conformal adhesion of wearable strain sensors onto the soft skin is another important consideration for noise-free and accurate strain monitoring.<sup>[190]</sup> The weak interfacial adhesion between wearable sensors and skin leads to their sliding and delamination from the skin. To date, several strategies, including pressure-sensitive adhesives,<sup>[234,235]</sup> gecko-inspired structures,<sup>[236,237]</sup> swellable microneedle arrays,<sup>[238,239]</sup> and ultrathin packaging<sup>[240,241]</sup> have been pursued to improve the skin adhesion. Nonetheless, high adhesion strength on the skin is still challenging, given its soft, irregular, rough, and textured structure. Drotlef et al. have recently addressed this by developing a flexible skin–adhesive film composed of PDMS microfibers decorated with vinylsiloxane tips.<sup>[190]</sup> Direct crosslinking of the viscous vinylsiloxane tips on the skin surface greatly enhanced the skin adhesion strength (up to 18 kPa) due to the excellent shape adaptation of microfiber tips to the multiscale roughness of the skin. Wearable strain sensors integrated with skin–adhesive composite microfibers showed amplified signal quality because of their conformal attachment to the skin.

Third, another key challenge in the design of wearable sensors is to achieve a high level of biocompatibility and health safety upon their prolonged application to the skin.<sup>[242]</sup> The majority of wearable strain sensors are made of polymeric films and planar structures, which in turn can prevent the circulation of the fresh air in the attached area and thereby can increase the chance of skin irritation, bacterial infection, and patients' discomfort.<sup>[242]</sup> To overcome this, limited attempts have been made to develop breathable wearable devices utilizing 3D microarchitectures, structured fiber films, and porous polymers.<sup>[154,190,243]</sup> A recent study has shown significant suppression of the skin inflammation by designing nanomesh, ultrathin, and gas-permeable wearable devices.<sup>[244]</sup> Therefore, the research focus should move toward the development of wearable strain sensors using more biocompatible and clinically acceptable materials.

Last but not least, along with the notable advancements in wearable strain sensors, considerable efforts have been made to develop other types of wearable electronic devices, including flexible wireless communication,<sup>[245–247]</sup> highly

stretchable energy storage and harvesting devices,<sup>[248–251]</sup> electronic circuits,<sup>[35,252,253]</sup> displays,<sup>[254,255]</sup> memories,<sup>[256,257]</sup> and interconnections.<sup>[258,259]</sup> However, it is still very challenging to achieve compact, fully functional, and reliable integration of all these components mainly because of the technical complexity in the manufacturing process.<sup>[1,260]</sup> Consequently, further research efforts are critically needed for device integration and digital manufacturing (e.g., 3D printing and laser micromachining) toward multifunctional wearable devices with greater functionalities and longer lifetime.<sup>[199,249]</sup> In another practical approach, wearable devices have been hybridized with custom-made commercial silicon-based electronic chips.<sup>[8,191,261–264]</sup> These miniaturized chips power the wearable devices, collect and calibrate the sensory information, and transmit the acquired data to a mobile device (e.g., computer, smartphone, and tablet) via wireless communication. For instance, an integrated smart glove system has been developed containing wearable strain sensors and a custom-made miniaturized electronic chip for data acquisition, calibration, and wireless communication.<sup>[8]</sup> In another example, Gao et al. integrated soft multimodal biosensors with a flexible printed circuit board (FPCB) made of a memory chip, rechargeable battery, microcontroller, and wireless communication module for sweat sensing and analysis.<sup>[261]</sup> Although there was a large mechanical mismatch between the FPCB and wearable biosensors and the skin, their miniaturized designs and compact integration have shown potentials in point-of-care devices.

## 9. Conclusions and Future Outlook

The recent technological advances in the development of stretchable and wearable strain sensors were summarized in this Review. Capacitive-type sensors offer excellent stretchability, linearity, and negligible hysteresis, but they have poor sensitivity. The sensitivity and stretchability of resistive-type sensors have been greatly improved through advanced materials and structural engineering. However, they often suffer from hysteresis and nonlinear electromechanical response. The drawbacks of stretchable optical strain sensors are their poor dynamic performance and long-term durability, and relatively slow response time. Therefore, several challenges associated with the design of high-performance, multidirectional, skin conformal, breathable, and integrated wearable strain sensors should be further addressed. Potential application areas while improving the present state-of-the-art sensing platform include body stimulators, wearable healthcare, assistive devices, smart surgical devices, drug delivery monitoring, as well as in artificial organ research. In addition, building multifunctional strain sensors will enhance biological understanding and will formulate novel and exciting hypotheses for the live-organisms investigation. Similarly, functional nanomaterial composites for soft sensing will help with biomechanics, veterinary care, and animal welfare in general.

## Acknowledgements

A.J. thanks the Max Planck Society and the Cyber Valley Research Grant for Soft Interfaces (Grant No. CyVy-RF-2019-08) for financial support.

## Conflict of Interest

The authors declare no conflict of interest.

## Author Contributions

H.S. and M.A. proposed the structure of the paper and drafted the initial manuscript. H.B. and A.J. wrote the “Soft Robotics and Neuromechanics” section. M.A. and N.R. wrote the “Applications of Stretchable Strain Sensors” and the “Conclusions and Future Outlook” sections. All authors further edited and adapted the manuscript. M.A. and H.S. prepared the revised manuscript. All authors approved the final version of the article.

## Keywords

composites, nanomaterials, polymers, soft robotics, wearable strain sensors

Received: March 14, 2020

Revised: April 14, 2020

Published online: June 11, 2020

- [1] M. Amjadi, K. U. Kyung, I. Park, M. Sitti, *Adv. Funct. Mater.* **2016**, 26, 1678.
- [2] Y. Cheng, R. Wang, J. Sun, L. Gao, *Adv. Mater.* **2015**, 27, 7365.
- [3] M. Zhang, C. Wang, Q. Wang, M. Jian, Y. Zhang, *ACS Appl. Mater. Interfaces* **2016**, 8, 20894.
- [4] S. Ryu, P. Lee, J. B. Chou, R. Xu, R. Zhao, A. J. Hart, S.-G. Kim, *ACS Nano* **2015**, 9, 5929.
- [5] Z. F. Liu, S. Fang, F. A. Moura, J. N. Ding, N. Jiang, J. Di, M. Zhang, X. Lepró, D. S. Galvão, C. S. Haines, N. Y. Yuan, S. G. Yin, D. W. Lee, R. Wang, H. Y. Wang, W. Lv, C. Dong, R. C. Zhang, M. J. Chen, Q. Yin, Y. T. Chong, R. Zhang, X. Wang, M. D. Lima, R. Ovalle-Robles, D. Qian, H. Lu, R. H. Baughman, *Science* **2015**, 349, 400.
- [6] M. Amjadi, M. Turan, C. P. Clementson, M. Sitti, *ACS Appl. Mater. Interfaces* **2016**, 8, 5618.
- [7] J. Di, S. Yao, Y. Ye, Z. Cui, J. Yu, T. K. Ghosh, Y. Zhu, Z. Gu, *ACS Nano* **2015**, 9, 9407.
- [8] M. Amjadi, A. Pichitpajongkit, S. Lee, S. Ryu, I. Park, *ACS Nano* **2014**, 8, 5154.
- [9] M. Amjadi, Y. J. Yoon, I. Park, *Nanotechnology* **2015**, 26, 375501.
- [10] Y. Yang, L. Shi, Z. Cao, R. Wang, J. Sun, *Adv. Funct. Mater.* **2019**, 29, 1807882.
- [11] L. Duan, D. R. D'hooge, L. Cardon, *Prog. Mater. Sci.* **2019**, 100617.
- [12] D. Rus, M. T. Tolley, *Nature* **2015**, 521, 467.
- [13] N. Lu, D. H. Kim, *Soft Robot.* **2014**, 1, 53.
- [14] J. Kim, M. Lee, H. J. Shim, R. Ghaffari, H. R. Cho, D. Son, Y. H. Jung, M. Soh, C. Choi, S. Jung, K. Chu, D. Jeon, S. T. Lee, J. H. Kim, S. H. Choi, T. Hyeon, D. H. Kim, *Nat. Commun.* **2014**, 5, 1.
- [15] R. Nur, N. Matsuhsa, Z. Jiang, M. O. G. Nayeem, T. Yokota, T. Someya, *Nano Lett.* **2018**, 18, 5610.
- [16] S.-R. Kim, J.-H. Kim, J.-W. Park, *ACS Appl. Mater. Interfaces* **2017**, 9, 26407.
- [17] H. Sourji, J. Yu, H. Jeon, J. W. Kim, C. M. Yang, N. H. You, B. J. Yang, *Carbon* **2017**, 120, 427.
- [18] H. Sourji, I. W. Nam, H. Jeon, H. K. Lee, *Compos. Sci. Technol.* **2015**, 121, 41.
- [19] D. Wang, B. Sheng, L. Peng, Y. Huang, Z. Ni, *Polymers* **2019**, 11, 1433.
- [20] J. Guo, B. Zhou, R. Zong, L. Pan, X. Li, X. Yu, C. Yang, L. Kong, Q. Dai, *ACS Appl. Mater. Interfaces* **2019**, 11, 33589.
- [21] J. Chen, Q. Yu, X. Cui, M. Dong, J. Zhang, C. Wang, J. Fan, Y. Zhu, Z. Guo, *J. Mater. Chem. C* **2019**, 7, 11710.
- [22] G. Ge, W. Huang, J. Shao, X. Dong, *J. Semicond.* **2018**, 39, 011012.
- [23] S. Seyedin, P. Zhang, M. Naebe, S. Qin, J. Chen, X. Wang, J. M. Razal, *Mater. Horizons* **2019**, 6, 219.
- [24] S. Gong, W. Cheng, *Adv. Electron. Mater.* **2017**, 3, 1600314.
- [25] D. C. Kim, H. J. Shim, W. Lee, J. H. Koo, D. Kim, *Adv. Mater.* **2019**, 1902743.
- [26] B. Zhu, S. Gong, W. Cheng, *Chem. Soc. Rev.* **2019**, 48, 1668.
- [27] J. Li, L. Fang, B. Sun, X. Li, S. H. Kang, *J. Electrochem. Soc.* **2020**, 167, 037561.
- [28] H. Zhao, K. O'Brien, S. Li, R. F. Shepherd, *Sci. Robot.* **2016**, 1, eaai7529.
- [29] R. L. Truby, M. Wehner, A. K. Grosskopf, D. M. Vogt, S. G. M. Uzel, R. J. Wood, J. A. Lewis, *Adv. Mater.* **2018**, 30, 1706383.
- [30] A. Frutiger, J. T. Muth, D. M. Vogt, Y. Mengüç, A. Campo, A. D. Valentine, C. J. Walsh, J. A. Lewis, *Adv. Mater.* **2015**, 27, 2440.
- [31] X. Liao, Z. Zhang, Z. Kang, F. Gao, Q. Liao, Y. Zhang, *Mater. Horizons* **2017**, 4, 502.
- [32] K. Song, S. H. Kim, S. Jin, S. Kim, S. Lee, J. S. Kim, J. M. Park, Y. Cha, *Sci. Rep.* **2019**, 9, 1.
- [33] Q. Liu, J. Chen, Y. Li, G. Shi, *ACS Nano* **2016**, 10, 7901.
- [34] Z. Yang, Y. Pang, X. L. Han, Y. Yang, Y. Yang, J. Ling, M. Jian, Y. Zhang, T. L. Ren, *ACS Nano* **2018**, 12, 9134.
- [35] J. Byun, Y. Lee, J. Yoon, B. Lee, E. Oh, S. Chung, T. Lee, K. J. Cho, J. Kim, Y. Hong, *Sci. Robot.* **2018**, 3, eaas9020.
- [36] S. Choi, K. Yoon, S. Lee, H. J. Lee, J. Lee, D. W. Kim, M. S. Kim, T. Lee, C. Pang, *Adv. Funct. Mater.* **2019**, 29, 1905808.
- [37] H. Liu, Qianming Li, S. Zhang, R. Yin, X. Liu, Y. He, K. Dai, C. Shan, J. Guo, C. Liu, C. Shen, X. Wang, Ning Wang, Z. Wang, Renbo Wei, Z. Guo, *J. Mater. Chem. C* **2018**, 6, 12121.
- [38] A. Leber, B. Cholst, J. Sandt, N. Vogel, M. Kolle, *Adv. Funct. Mater.* **2019**, 29, 1802629.
- [39] W. Peng, H. Wu, *Adv. Opt. Mater.* **2019**, 7, 1900329.
- [40] C. Wang, K. Xia, H. Wang, X. Liang, Z. Yin, Y. Zhang, *Adv. Mater.* **2019**, 31, 1801072.
- [41] Z. Lou, L. Wang, G. Shen, *Adv. Mater. Technol.* **2018**, 3, 1800444.
- [42] J. Gu, D. Kwon, J. Ahn, I. Park, *ACS Appl. Mater. Interfaces* **2020**, 12, 10908.
- [43] Y. Zou, P. Tan, B. Shi, H. Ouyang, D. Jiang, Z. Liu, H. Li, M. Yu, C. Wang, X. Qu, L. Zhao, Y. Fan, Z. L. Wang, Z. Li, *Nat. Commun.* **2019**, 10, 1.
- [44] X. Chen, K. Parida, J. Wang, J. Xiong, M. F. Lin, J. Shao, P. S. Lee, *ACS Appl. Mater. Interfaces* **2017**, 9, 42200.
- [45] G. Zhao, Y. Zhang, N. Shi, Z. Liu, X. Zhang, M. Wu, C. Pan, H. Liu, L. Li, Z. L. Wang, *Nano Energy* **2019**, 59, 302.
- [46] Y. Cheng, D. Wu, S. Hao, Y. Jie, X. Cao, N. Wang, Z. L. Wang, *Nano Energy* **2019**, 64, 103907.
- [47] C. Dagdeviren, P. Joe, O. L. Tuzman, K. Il Park, K. J. Lee, Y. Shi, Y. Huang, J. A. Rogers, *Extrem. Mech. Lett.* **2016**, 9, 269.
- [48] C. Lu, J. Chen, T. Jiang, G. Gu, W. Tang, Z. L. Wang, *Adv. Mater. Technol.* **2018**, 3, 1800021.
- [49] H. Wang, D. Li, W. Zhong, L. Xu, T. Jiang, Z. L. Wang, *ACS Appl. Mater. Interfaces* **2019**, 11, 34251.
- [50] M. T. Almansoori, X. Li, L. Zheng, *Curr. Smart Mater.* **2019**, 4, 3.
- [51] W. Paosangthong, R. Torah, S. Beeby, *Nano Energy* **2019**, 55, 401.
- [52] S. Huang, G. He, C. Yang, J. Wu, C. Guo, T. Hang, B. Li, C. Yang, D. Liu, H.-J. Chen, Q. Wu, X. Gui, S. Deng, Y. Zhang, F. Liu, X. Xie, *ACS Appl. Mater. Interfaces* **2019**, 11, 1294.
- [53] J. Shintake, E. Piskarev, S. H. Jeong, D. Floreano, *Adv. Mater. Technol.* **2018**, 3, 1700284.

- [54] J. F. Christ, N. Aliheidari, A. Ameli, P. Pötschke, *Mater. Des.* **2017**, *131*, 394.
- [55] J. Song, Y. Tan, Z. Chu, M. Xiao, G. Li, Z. Jiang, J. Wang, T. Hu, *ACS Appl. Mater. Interfaces* **2019**, *11*, 1283.
- [56] J. Lee, S. Pyo, D. Kwon, E. Jo, W. Kim, J. Kim, *Small* **2019**, *15*, 1805120.
- [57] J. Wu, Z. Ma, Z. Hao, J. T. Zhang, P. Sun, M. Zhang, Y. Liu, Y. Cheng, Y. Li, B. Zhong, T. Zhang, L. Xia, W. Yao, X. Huang, H. Wang, H. Liu, F. Yan, C. E. Hsu, G. Xing, *ACS Appl. Nano Mater.* **2019**, *2*, 750.
- [58] J. Zhou, X. Xu, Y. Xin, G. Lubineau, *Adv. Funct. Mater.* **2018**, *28*, 1705591.
- [59] S. Wu, S. Peng, Z. J. Han, H. Zhu, C. H. Wang, *ACS Appl. Mater. Interfaces* **2018**, *10*, 36312.
- [60] B. Liang, Z. Lin, W. Chen, Z. He, J. Zhong, H. Zhu, Z. Tang, X. Gui, *Nanoscale* **2018**, *10*, 13599.
- [61] T. Yamada, Y. Hayamizu, Y. Yamamoto, Y. Yomogida, A. Izadi-Najafabadi, D. N. Futaba, K. Hata, *Nat. Nanotechnol.* **2011**, *6*, 296.
- [62] Z. He, G. Zhou, J. H. Byun, S. K. Lee, M. K. Um, B. Park, T. Kim, S. B. Lee, T. W. Chou, *Nanoscale* **2019**, *11*, 5884.
- [63] Y. Gao, F. Guo, P. Cao, J. Liu, D. Li, J. Wu, N. Wang, Y. Su, Y. Zhao, *ACS Nano* **2020**, *14*, 3442.
- [64] Y. Wang, J. Hao, Z. Huang, G. Zheng, K. Dai, C. Liu, C. Shen, *Carbon N. Y.* **2018**, *126*, 360.
- [65] M. Xu, J. Qi, F. Li, Y. Zhang, *Nanoscale* **2018**, *10*, 5264.
- [66] G. Shi, Z. Zhao, J.-H. Pai, I. Lee, L. Zhang, C. Stevenson, K. Ishara, R. Zhang, H. Zhu, J. Ma, *Adv. Funct. Mater.* **2016**, *26*, 7614.
- [67] S. Wu, R. B. Ladani, J. Zhang, K. Ghorbani, X. Zhang, A. P. Mouritz, A. J. Kinloch, C. H. Wang, *ACS Appl. Mater. Interfaces* **2016**, *8*, 24853.
- [68] Y. Li, B. Zhou, G. Zheng, X. Liu, T. Li, C. Yan, C. Cheng, K. Dai, C. Liu, C. Shen, Z. Guo, *J. Mater. Chem. C* **2018**, *6*, 2258.
- [69] Y. Zheng, Y. Li, K. Dai, Y. Wang, G. Zheng, C. Liu, C. Shen, *Compos. Sci. Technol.* **2018**, *156*, 276.
- [70] S. W. Lee, J. J. Park, B. H. Park, S. C. Mun, Y. T. Park, K. Liao, T. S. Seo, W. J. Hyun, O. O. Park, *ACS Appl. Mater. Interfaces* **2017**, *9*, 11176.
- [71] H. Xu, Y. Lv, D. Qiu, Y. Zhou, H. Zeng, Y. Chu, *Nanoscale* **2019**, *11*, 1570.
- [72] K.-H. Kim, N.-S. Jang, S.-H. Ha, J. H. Cho, J.-M. Kim, *Small* **2018**, *14*, 1704232.
- [73] J. H. Cho, S. H. Ha, J. M. Kim, *Nanotechnology* **2018**, *29*, 155501.
- [74] M. D. Ho, Y. Ling, L. W. Yap, Y. Wang, D. Dong, Y. Zhao, W. Cheng, *Adv. Funct. Mater.* **2017**, *27*, 1700845.
- [75] S. Duan, Z. Wang, L. Zhang, J. Liu, C. Li, *Adv. Mater. Technol.* **2018**, *3*, 1800020.
- [76] B. Tian, W. Yao, P. Zeng, X. Li, H. Wang, L. Liu, Y. Feng, C. Luo, W. Wu, *J. Mater. Chem. C* **2019**, *7*, 809.
- [77] W. Zhong, C. Liu, C. Xiang, Y. Jin, M. Li, K. Liu, Q. Liu, Y. Wang, G. Sun, D. Wang, *ACS Appl. Mater. Interfaces* **2017**, *9*, 42058.
- [78] K. K. Kim, S. Hong, H. M. Cho, J. Lee, Y. D. Suh, J. Ham, S. H. Ko, *Nano Lett.* **2015**, *15*, 5240.
- [79] I. You, B. Kim, J. Park, K. Koh, S. Shin, S. Jung, U. Jeong, *Adv. Mater.* **2016**, *28*, 6359.
- [80] X. Shi, H. Wang, X. Xie, Q. Xue, J. Zhang, S. Kang, C. Wang, J. Liang, Y. Chen, *ACS Nano* **2019**, *13*, 649.
- [81] Y. Cai, J. Shen, G. Ge, Y. Zhang, W. Jin, W. Huang, J. Shao, J. Yang, X. Dong, *ACS Nano* **2018**, *12*, 56.
- [82] D. Yun Choi, M. Hyeong Kim, Y. Suk Oh, S.-H. Jung, J. Hee Jung, H. Jin Sung, H. Woo Lee, H. Moon Lee, *ACS Publ.* **2016**, *9*, 1770.
- [83] S. Chen, H. Liu, S. Liu, P. Wang, S. Zeng, L. Sun, L. Liu, *ACS Appl. Mater. Interfaces* **2018**, *10*, 4305.
- [84] T. Yan, Z. Wang, Y. Q. Wang, Z. J. Pan, *Mater. Des.* **2018**, *143*, 214.
- [85] S. Chen, Y. Wei, X. Yuan, Y. Lin, L. Liu, *J. Mater. Chem. C* **2016**, *4*, 4304.
- [86] S. Chen, Y. Wei, S. Wei, Y. Lin, L. Liu, *ACS Appl. Mater. Interfaces* **2016**, *8*, 25563.
- [87] J. Shi, X. Li, H. Cheng, Z. Liu, L. Zhao, T. Yang, Z. Dai, Z. Cheng, E. Shi, L. Yang, Z. Zhang, A. Cao, H. Zhu, Y. Fang, *Adv. Funct. Mater.* **2016**, *26*, 2078.
- [88] J. Shi, J. Hu, Z. Dai, W. Zhao, P. Liu, L. Zhao, Y. Guo, T. Yang, L. Zou, K. Jiang, H. Li, Y. Fang, *Carbon N. Y.* **2017**, *123*, 786.
- [89] S. Chen, R. Wu, P. Li, Q. Li, Y. Gao, B. Qian, F. Xuan, *ACS Appl. Mater. Interfaces* **2018**, *10*, 37760.
- [90] L. M. Zhang, Y. He, S. Cheng, H. Sheng, K. Dai, W. J. Zheng, M. X. Wang, Z. S. Chen, Y. M. Chen, Z. Suo, *Small* **2019**, *15*, 1804651.
- [91] Y. Cai, J. Shen, Z. Dai, X. Zang, Q. Dong, G. Guan, L.-J. Li, W. Huang, X. Dong, *Adv. Mater.* **2017**, *29*, 1606411.
- [92] X. Guo, Y. Huang, Y. Zhao, L. Mao, L. Gao, W. Pan, Y. Zhang, P. Liu, *Smart Mater. Struct.* **2017**, *26*, 095017.
- [93] Q. Li, Z. Ullah, W. Li, Y. Guo, J. Xu, R. Wang, Q. Zeng, M. Chen, C. Liu, L. Liu, *Small* **2016**, *12*, 5058.
- [94] Z. Wang, H. Zhou, W. Chen, Q. Li, B. Yan, X. Jin, A. Ma, H. Liu, W. Zhao, *ACS Appl. Mater. Interfaces* **2018**, *10*, 14045.
- [95] F. Zhang, S. Wu, S. Peng, Z. Sha, C. H. Wang, *Compos. Sci. Technol.* **2019**, *172*, 7.
- [96] X. Fan, N. Wang, F. Yan, J. Wang, W. Song, Z. Ge, *Adv. Mater. Technol.* **2018**, *3*, 1800030.
- [97] T. Wang, Y. Zhang, Q. Liu, W. Cheng, X. Wang, L. Pan, B. Xu, H. Xu, *Adv. Funct. Mater.* **2018**, *28*, 1705551.
- [98] Y. Ding, W. Xu, W. Wang, H. Fong, Z. Zhu, *ACS Appl. Mater. Interfaces* **2017**, *9*, 30014.
- [99] Y. He, Q. Gui, Y. Wang, Z. Wang, S. Liao, Y. Wang, *Small* **2018**, *14*, 1800394.
- [100] S. Liu, R. Zheng, S. Chen, Y. Wu, H. Liu, P. Wang, Z. Deng, L. Liu, *J. Mater. Chem. C* **2018**, *6*, 4183.
- [101] J. Eom, R. Jaisutti, H. Lee, W. Lee, J.-S. Heo, J.-Y. Lee, S. K. Park, Y.-H. Kim, *ACS Appl. Mater. Interfaces* **2017**, *9*, 10190.
- [102] D. Cho, J. Park, J. Kim, T. Kim, J. Kim, I. Park, S. Jeon, *ACS Appl. Mater. Interfaces* **2017**, *9*, 17369.
- [103] Y. Zheng, Y. Li, Z. Li, Y. Wang, K. Dai, G. Zheng, C. Liu, C. Shen, *Compos. Sci. Technol.* **2017**, *139*, 64.
- [104] Y. Wu, I. Karakurt, L. Beker, Y. Kubota, R. Xu, K. Y. Ho, S. Zhao, J. Zhong, M. Zhang, X. Wang, L. Lin, *Sens. Actuators A Phys.* **2018**, *279*, 46.
- [105] J. Sun, Y. Zhao, Z. Yang, J. Shen, E. Cabrera, M. J. Lertola, W. Yang, D. Zhang, A. Benatar, J. M. Castro, D. Wu, L. J. Lee, *Nanotechnology* **2018**, *29*, 355304.
- [106] Y. Wang, Y. Wang, Y. Yang, *Adv. Energy Mater.* **2018**, *8*, 1800961.
- [107] S.-J. Park, J. Kim, M. Chu, M. Khine, *Adv. Mater. Technol.* **2016**, *1*, 1600053.
- [108] X. Wang, J. Li, H. Song, H. Huang, J. Gou, *ACS Appl. Mater. Interfaces* **2018**, *10*, 7371.
- [109] S. Wang, P. Xiao, Y. Liang, J. Zhang, Y. Huang, S. Wu, S. W. Kuo, T. Chen, *J. Mater. Chem. C* **2018**, *6*, 5140.
- [110] B. Nie, X. Li, J. Shao, X. Li, H. Tian, D. Wang, Q. Zhang, B. Lu, *ACS Appl. Mater. Interfaces* **2017**, *9*, 40681.
- [111] J. Zhou, H. Yu, X. Xu, F. Han, G. Lubineau, *ACS Appl. Mater. Interfaces* **2017**, *9*, 4835.
- [112] X. Ye, Z. Yuan, H. Tai, W. Li, X. Du, Y. Jiang, *J. Mater. Chem. C* **2017**, *5*, 7746.
- [113] G. Li, K. Dai, M. Ren, Y. Wang, G. Zheng, C. Liu, C. Shen, *J. Mater. Chem. C* **2018**, *6*, 6575.
- [114] X. Zhou, L. Zhu, L. Fan, H. Deng, Q. Fu, *ACS Appl. Mater. Interfaces* **2018**, *10*, 31655.
- [115] S. Han, C. Liu, H. Xu, D. Yao, K. Yan, H. Zheng, H.-J. Chen, X. Gui, S. Chu, C. Liu, *npj Flex. Electron.* **2018**, *2*, 1.
- [116] T. Yang, X. Li, X. Jiang, S. Lin, J. Lao, J. Shi, Z. Zhen, Z. Li, H. Zhu, *Mater. Horizons* **2016**, *3*, 248.



- [117] F. Han, J. Li, S. Zhao, Y. Zhang, W. Huang, G. Zhang, R. Sun, C. P. Wong, *J. Mater. Chem. C* **2017**, 5, 10167.
- [118] G. H. Lim, N. E. Lee, B. Lim, *J. Mater. Chem. C* **2016**, 4, 5642.
- [119] S. Wang, K. Chen, M. Wang, H. Li, G. Chen, J. Liu, L. Xu, Y. Jian, C. Meng, X. Zhang, S. Liu, C. Yin, Z. Wang, P. Du, S. Qu, C. W. Leung, *J. Mater. Chem. C* **2018**, 6, 4737.
- [120] L. Wang, J. Luo, Y. Chen, L. Lin, X. Huang, H. Xue, J. Gao, *ACS Appl. Mater. Interfaces* **2019**, 11, 17774.
- [121] Z. Cao, R. Wang, T. He, F. Xu, J. Sun, *ACS Appl. Mater. Interfaces* **2018**, 10, 14087.
- [122] J. Ren, X. Du, W. Zhang, M. Xu, *RSC Adv.* **2017**, 7, 22619.
- [123] L. Wang, Y. Chen, L. Lin, H. Wang, X. Huang, H. Xue, J. Gao, *Chem. Eng. J.* **2019**, 362, 89.
- [124] M. Abshirini, M. Charara, Y. Liu, M. Saha, M. C. Altan, *Adv. Eng. Mater.* **2018**, 20, 1800425.
- [125] Q. Li, J. Li, D. Tran, C. Luo, Y. Gao, C. Yu, F. Xuan, *J. Mater. Chem. C* **2017**, 5, 11092.
- [126] X. Liu, C. Tang, X. Du, S. Xiong, S. Xi, Y. Liu, X. Shen, Q. Zheng, Z. Wang, Y. Wu, A. Horner, J. K. Kim, *Mater. Horizons* **2017**, 4, 477.
- [127] Z. Wang, Q. Zhang, Y. Yue, J. Xu, W. Xu, X. Sun, Y. Chen, J. Jiang, Y. Liu, *Nanotechnology* **2019**, 30, 345501.
- [128] X. Li, H. Hu, T. Hua, B. Xu, S. Jiang, *Nano Res.* **2018**, 11, 5799.
- [129] L. Q. Tao, D. Y. Wang, H. Tian, Z. Y. Ju, Y. Liu, Y. Pang, Y. Q. Chen, Y. Yang, T. L. Ren, *Nanoscale* **2017**, 9, 8266.
- [130] C. Liu, S. Han, H. Xu, J. Wu, C. Liu, *ACS Appl. Mater. Interfaces* **2018**, 10, 31716.
- [131] P. Cataldi, S. Dussoni, L. Ceseracciu, M. Maggiali, L. Natale, G. Metta, A. Athanassiou, I. S. Bayer, *Adv. Sci.* **2018**, 5, 1700587.
- [132] H. Yang, X. F. Yao, Z. Zheng, L. H. Gong, L. Yuan, Y. N. Yuan, Y. H. Liu, *Compos. Sci. Technol.* **2018**, 167, 371.
- [133] P. Liu, W. Pan, Y. Liu, J. Liu, W. Xu, X. Guo, C. Liu, Y. Zhang, Y. Ge, Y. Huang, *Compos. Sci. Technol.* **2018**, 159, 42.
- [134] O. Atalay, A. Atalay, J. Gafford, H. Wang, R. Wood, C. Walsh, *Adv. Mater. Technol.* **2017**, 2, 1700081.
- [135] H. Wu, Q. Liu, W. Du, C. Li, G. Shi, *ACS Appl. Mater. Interfaces* **2018**, 10, 3895.
- [136] X. Wu, Y. Han, X. Zhang, C. Lu, *ACS Appl. Mater. Interfaces* **2016**, 8, 9936.
- [137] X. Wang, H. Sun, X. Yue, Y. Yu, G. Zheng, K. Dai, C. Liu, C. Shen, *Compos. Sci. Technol.* **2018**, 168, 126.
- [138] Y. Zhou, P. Zhan, M. Ren, G. Zheng, K. Dai, L. Mi, C. Liu, C. Shen, *ACS Appl. Mater. Interfaces* **2019**, 11, 7405.
- [139] Z. Wang, X. Guan, H. Huang, H. Wang, W. Lin, Z. Peng, *Adv. Funct. Mater.* **2019**, 29, 1807569.
- [140] J. Z. Gul, M. Sajid, K. H. Choi, *J. Mater. Chem. C* **2019**, 7, 4692.
- [141] S. Lin, X. Zhao, X. Jiang, A. Wu, H. Ding, Y. Zhong, J. Li, J. Pan, B. Liu, H. Zhu, *Small* **2019**, 15, 1900848.
- [142] S. R. Larimi, H. Rezaei Nejad, M. Oyatsi, A. O'Brien, M. Hoorfar, H. Najjaran, *Sens. Actuators A Phys.* **2018**, 271, 182.
- [143] H. Souri, D. Bhattacharyya, *Sens. Actuators A Phys.* **2019**, 285, 142.
- [144] H. Souri, D. Bhattacharyya, *Mater. Des.* **2018**, 154, 217.
- [145] H. Souri, D. Bhattacharyya, *J. Mater. Chem. C* **2018**, 6, 10524.
- [146] H. Souri, D. Bhattacharyya, *ACS Appl. Mater. Interfaces* **2018**, 10, 20845.
- [147] P. Cataldi, L. Ceseracciu, A. Athanassiou, I. S. Bayer, *ACS Appl. Mater. Interfaces* **2017**, 9, 13825.
- [148] M. Zhang, C. Wang, H. Wang, M. Jian, X. Hao, Y. Zhang, *Adv. Funct. Mater.* **2017**, 27, 1604795.
- [149] C. Wang, X. Li, E. Gao, M. Jian, K. Xia, Q. Wang, Z. Xu, T. Ren, Y. Zhang, *Adv. Mater.* **2016**, 28, 6640.
- [150] M. Zahid, E. L. Papadopoulou, A. Athanassiou, I. S. Bayer, *Mater. Des.* **2017**, 135, 213.
- [151] J. Guo, M. Niu, C. Yang, *Optica* **2017**, 4, 1285.
- [152] C. Wang, K. Xia, M. Jian, H. Wang, M. Zhang, Y. Zhang, *J. Mater. Chem. C* **2017**, 5, 7604.
- [153] J. Y. Kim, S. Ji, S. Jung, B. H. Ryu, H. S. Kim, S. S. Lee, Y. Choi, S. Jeong, *Nanoscale* **2017**, 9, 11035.
- [154] B. Sun, R. N. McCay, S. Goswami, Y. Xu, C. Zhang, Y. Ling, J. Lin, Z. Yan, *Adv. Mater.* **2018**, 30, 1804327.
- [155] Y. Miao, L. Wan, X. Ling, B. Chen, L. Pan, Y. Gao, *ACS Appl. Electron. Mater.* **2020**, 2, 855.
- [156] Y. Gao, C. Lu, Y. Guohui, J. Sha, J. Tan, F. Xuan, *Nanotechnology* **2019**, 30, 325502.
- [157] S. Hayashi, Y. Nakajima, M. Terakawa, *Opt. Mater. Express* **2019**, 9, 2672.
- [158] Y. Gao, Q. Li, R. Wu, J. Sha, Y. Lu, F. Xuan, *Adv. Funct. Mater.* **2019**, 29, 1806786.
- [159] J. Ren, C. Wang, X. Zhang, T. Carey, K. Chen, Y. Yin, F. Torrisi, *Carbon N. Y.* **2017**, 111, 622.
- [160] G. Cai, M. Yang, Z. Xu, J. Liu, B. Tang, X. Wang, *Chem. Eng. J.* **2017**, 325, 396.
- [161] C. Wang, M. Zhang, K. Xia, X. Gong, H. Wang, Z. Yin, B. Guan, Y. Zhang, *ACS Appl. Mater. Interfaces* **2017**, 9, 13331.
- [162] S. J. Kim, W. Song, Y. Yi, B. K. Min, S. Mondal, K.-S. An, C.-G. Choi, *ACS Appl. Mater. Interfaces* **2018**, 10, 3921.
- [163] B. Yin, Y. Wen, T. Hong, Z. Xie, G. Yuan, Q. Ji, H. Jia, *ACS Appl. Mater. Interfaces* **2017**, 9, 32054.
- [164] O. Atalay, A. Atalay, J. Gafford, C. Walsh, *Adv. Mater. Technol.* **2018**, 3, 1700237.
- [165] J. Guo, X. Liu, N. Jiang, A. K. Yetisen, H. Yuk, C. Yang, A. Khademhosseini, X. Zhao, S.-H. Yun, *Adv. Mater.* **2016**, 28, 10244.
- [166] Y. Qu, T. Nguyen-Dang, A. G. Page, W. Yan, T. Das Gupta, G. M. Rotaru, R. M. Rossi, V. D. Favrod, N. Bartolomei, F. Sorin, *Adv. Mater.* **2018**, 30, 1707251.
- [167] B. Wright, D. M. Vogt, R. J. Wood, A. Jusufi, in *IEEE International Conference on Soft Robotics*, Institute of Electrical and Electronics Engineers Inc., Seoul, South Korea **2019**, pp. 367–371.
- [168] M. D. Dickey, *Adv. Mater.* **2017**, 29, 1606425.
- [169] B. Ma, C. Xu, J. Chi, J. Chen, C. Zhao, H. Liu, *Adv. Funct. Mater.* **2019**, 29, 1901370.
- [170] M. Kim, H. Alrowais, O. Brand, *Adv. Electron. Mater.* **2018**, 4, 1700434.
- [171] L. Dejace, N. Laubeuf, I. Furfaro, S. P. Lacour, *Adv. Intell. Syst.* **2019**, 1, 1900079.
- [172] Y. Huang, Y. Zhao, Y. Wang, X. Guo, Y. Zhang, P. Liu, C. Liu, Y. Zhang, *Smart Mater. Struct.* **2018**, 27, 035013.
- [173] Q. Li, K. Wang, Y. Gao, J. P. Tan, R. Y. Wu, F. Z. Xuan, *Appl. Phys. Lett.* **2018**, 112, 263501.
- [174] J. Zhou, X. Xu, H. Yu, G. Lubineau, *Nanoscale* **2017**, 9, 604.
- [175] C. J. Lee, K. H. Park, C. J. Han, M. S. Oh, B. You, Y. S. Kim, J. W. Kim, *Sci. Rep.* **2017**, 7, 1.
- [176] H. Jeon, S. K. Hong, M. S. Kim, S. J. Cho, G. Lim, *ACS Appl. Mater. Interfaces* **2017**, 9, 41712.
- [177] X. Liao, Z. Zhang, Q. Liang, Q. Liao, Y. Zhang, *ACS Appl. Mater. Interfaces* **2017**, 9, 4151.
- [178] J. Tolvanen, J. Hannu, H. Jantunen, *Sci. Rep.* **2018**, 8, 1.
- [179] Y. Wu, H. Liu, S. Chen, X. Dong, P. Wang, S. Liu, Y. Lin, Y. Wei, L. Liu, *ACS Appl. Mater. Interfaces* **2017**, 9, 20098.
- [180] J. Lee, S. Kim, J. Lee, D. Yang, B. C. Park, S. Ryu, I. Park, *Nanoscale* **2014**, 6, 11932.
- [181] Z. Tang, S. Jia, F. Wang, C. Bian, Y. Chen, Y. Wang, B. Li, *ACS Appl. Mater. Interfaces* **2018**, 10, 6624.
- [182] Y. Wang, Y. Jia, Y. Zhou, Y. Wang, G. Zheng, K. Dai, C. Liu, C. Shen, *J. Mater. Chem. C* **2018**, 6, 8160.
- [183] J. Ma, P. Wang, H. Chen, S. Bao, W. Chen, H. Lu, *ACS Appl. Mater. Interfaces* **2019**, 11, 8527.

- [184] C. Luo, J. Jia, Y. Gong, Z. Wang, Q. Fu, C. Pan, *ACS Appl. Mater. Interfaces* **2017**, *9*, 19955.
- [185] C. B. Cooper, K. Arutselvan, Y. Liu, D. Armstrong, Y. Lin, M. R. Khan, J. Genzer, M. D. Dickey, *Adv. Funct. Mater.* **2017**, *27*, 1605630.
- [186] L. Ling, F. Liu, J. Li, G. Zhang, R. Sun, C.-P. Wong, *Macromol. Chem. Phys.* **2018**, *219*, 1800369.
- [187] H. Park, D. S. Kim, S. Y. Hong, C. Kim, J. Y. Yun, S. Y. Oh, S. W. Jin, Y. R. Jeong, G. T. Kim, J. S. Ha, *Nanoscale* **2017**, *9*, 7631.
- [188] L. Lu, Y. Zhou, J. Pan, T. Chen, Y. Hu, G. Zheng, K. Dai, C. Liu, C. Shen, X. Sun, H. Peng, *ACS Appl. Mater. Interfaces* **2019**, *11*, 4345.
- [189] Z. Wang, Y. Huang, J. Sun, Y. Huang, H. Hu, R. Jiang, W. Gai, G. Li, C. Zhi, *ACS Appl. Mater. Interfaces* **2016**, *8*, 24837.
- [190] D.-M. Drotleff, M. Amjadi, M. Yunusa, M. Sitti, *Adv. Mater.* **2017**, *29*, 1701353.
- [191] Z. Liu, D. Qi, G. Hu, H. Wang, Y. Jiang, G. Chen, Y. Luo, X. J. Loh, B. Liedberg, X. Chen, *Adv. Mater.* **2018**, *30*, 1704229.
- [192] J. Zhang, Y. Cao, M. Qiao, L. Ai, K. Sun, Q. Mi, S. Zang, Y. Zuo, X. Yuan, Q. Wang, *Sens. Actuators A Phys.* **2018**, *274*, 132.
- [193] S. Wan, Z. Zhu, K. Yin, S. Su, H. Bi, T. Xu, H. Zhang, Z. Shi, L. He, L. Sun, *Small Methods* **2018**, *2*, 1700374.
- [194] S. Patel, H. Park, P. Bonato, L. Chan, M. Rodgers, *J. Neuroeng. Rehabil.* **2012**, *9*, 21.
- [195] C. Larson, B. Peele, S. Li, S. Robinson, M. Totaro, L. Beccai, B. Mazzolai, R. Shepherd, *Science* **2016**, *351*, 1071.
- [196] S. Cheng, Y. S. Narang, C. Yang, Z. Suo, R. D. Howe, *Adv. Mater. Interfaces* **2019**, *6*, 1900985.
- [197] M. Amjadi, M. Sitti, *Adv. Sci.* **2018**, *5*, 1800239.
- [198] A. C. McConnell, M. Vallejo, R. C. Moiola, F. L. Brasil, N. Secciani, M. P. Nemitz, C. P. Riquart, D. W. Corne, P. A. Vargas, A. A. Stokes, *Front. Mech. Eng.* **2017**, *3*, 3.
- [199] A. Zolfagharian, A. Kaynak, A. Kouzani, *Mater. Des.* **2020**, *188*, 108411.
- [200] J. C. Yeo, H. K. Yap, W. Xi, Z. Wang, C.-H. Yeow, C. T. Lim, *Adv. Mater. Technol.* **2016**, *1*, 1600018.
- [201] Y. R. Jeong, H. Park, S. W. Jin, S. Y. Hong, S.-S. Lee, J. S. Ha, *Adv. Funct. Mater.* **2015**, *25*, 4228.
- [202] D. Kang, P. V. Pikhitsa, Y. W. Choi, C. Lee, S. S. Shin, L. Piao, B. Park, K. Y. Suh, T. Il Kim, M. Choi, *Nature* **2014**, *516*, 222.
- [203] H. Banerjee, M. Suhail, H. Ren, *Biomimetics* **2018**, *3*, 15.
- [204] S. Xu, D. M. Vogt, W.-H. Hsu, J. Osborne, T. Walsh, J. R. Foster, S. K. Sullivan, V. C. Smith, A. W. Rousing, E. C. Goldfield, R. J. Wood, *Adv. Funct. Mater.* **2019**, *29*, 1807058.
- [205] J. T. Muth, D. M. Vogt, R. L. Truby, Y. Mengüç, D. B. Kolesky, R. J. Wood, J. A. Lewis, *Adv. Mater.* **2014**, *26*, 6307.
- [206] X. Wang, L. Dong, H. Zhang, R. Yu, C. Pan, Z. L. Wang, *Adv. Sci.* **2015**, *2*, 1500169.
- [207] A. Atalay, V. Sanchez, O. Atalay, D. M. Vogt, F. Haufe, R. J. Wood, C. J. Walsh, *Adv. Mater. Technol.* **2017**, *2*, 1700136.
- [208] H. Banerjee, H. Ren, in *Electromagnetic Actuation and Sensing in Medical Robotics* (Eds: H. Ren, J. Sun), Springer, Singapore **2018**, pp. 43–72.
- [209] H. Banerjee, G. Ponraj, S. K. Kirthika, M. V. Suman, C. M. Lim, H. Ren, *J. Med. Device.* **2019**, *13*, 044503.
- [210] H. Banerjee, T. K. Li, G. Ponraj, S. K. Kirthika, C. M. Lim, H. Ren, *J. Mech. Robot.* **2020**, *12*, 031010.
- [211] J. Aguilar, D. I. Goldman, *Nat. Phys.* **2016**, *12*, 278.
- [212] J. A. Nyakatura, K. Melo, T. Horvat, K. Karakasiliotis, V. R. Allen, A. Andikfar, E. Andrada, P. Arnold, J. Lauströer, J. R. Hutchinson, M. S. Fischer, A. J. Ijspeert, *Nature* **2019**, *565*, 351.
- [213] S. Sponberg, *Phys. Today* **2017**, *70*, 35.
- [214] N. Gravish, G. V. Lauder, *J. Exp. Biol.* **2018**, *221*, jeb138438.
- [215] J. T. Reeder, T. Kang, S. Rains, W. Voit, *Adv. Mater.* **2018**, *30*, 1706733.
- [216] A. Jusufi, D. M. Vogt, R. J. Wood, G. V. Lauder, *Soft Robot.* **2017**, *4*, 202.
- [217] J. C. Liao, D. N. Beal, G. V. Lauder, M. S. Triantafyllou, *J. Exp. Biol.* **2003**, *206*, 1059.
- [218] Y. Mengüç, Y.-L. Park, H. Pei, D. Vogt, P. M. Aubin, E. Winchell, L. Fluke, L. Stirling, R. J. Wood, C. J. Walsh, *Int. J. Rob. Res.* **2014**, *33*, 1748.
- [219] J. Kim, G. Lee, R. Heimgartner, D. A. Revi, N. Karavas, D. Nathanson, I. Galiana, A. Eckert-Erdheim, P. Murphy, D. Perry, N. Menard, D. K. Choe, P. Malcolm, C. J. Walsh, *Science* **2019**, *365*, 668.
- [220] J. Aguilar, T. Zhang, F. Qian, M. Kingsbury, B. McInroe, N. Mazouchova, C. Li, R. Maladen, C. Gong, M. Travers, R. L. Hattton, H. Choset, P. B. Umbanhowar, D. I. Goldman, *Rep. Prog. Phys.* **2016**, *79*, 110001.
- [221] J. A. Nirody, J. Jinn, T. Libby, R. J. Lee, A. Jusufi, D. L. Hu, R. J. Full, *Curr. Biol.* **2018**, *28*, 4046.
- [222] M. Asadnia, A. G. P. Kottapalli, K. D. Karavitaki, M. E. Warkiani, J. Miao, D. P. Corey, M. Triantafyllou, *Sci. Rep.* **2016**, *6*, 1.
- [223] A. G. P. Kottapalli, M. Bora, M. Asadnia, J. Miao, S. S. Venkatraman, M. Triantafyllou, *Sci. Rep.* **2016**, *6*, 1.
- [224] H. S. Shin, T. Kim, S. Bergbreiter, Y. L. Park, in *RoboSoft 2019–2019 IEEE International Conference on Soft Robotics*, Institute of Electrical and Electronics Engineers Inc., Seoul, South Korea **2019**, pp. 611–616.
- [225] M. E. McConney, N. Chen, D. Lu, H. A. Hu, S. Coombs, C. Liu, V. V. Tsukruk, *Soft Matter* **2009**, *5*, 292.
- [226] N. Chen, C. Tucker, J. M. Engel, Y. Yang, S. Pandya, C. Liu, *J. Microelectromech. Syst.* **2007**, *16*, 999.
- [227] R. Wolf, A. Jusufi, D. M. Vogt, G. V. Lauder, *Biospir. Biomim.* **2020**, <https://doi.org/10.1088/1748-3190/ab8d0f>.
- [228] Z. Liu, D. Qi, W. R. Leow, J. Yu, M. Xiloyannis, L. Cappello, Y. Liu, B. Zhu, Y. Jiang, G. Chen, L. Masia, B. Liedberg, X. Chen, *Adv. Mater.* **2018**, *30*, 1707285.
- [229] M. Nankali, N. M. Nouri, M. Navidbakhsh, N. Geran Malek, M. A. Amindehghan, A. Montazeri Shahtoori, M. Karimi, M. Amjadi, *J. Mater. Chem. C* **2020**, <https://doi.org/10.1039/d0tc00373e>.
- [230] P. Ahuja, S. Akiyama, S. K. Ujjain, R. Kukobat, F. Vallejos-Burgos, R. Futamura, T. Hayashi, M. Kimura, D. Tomanek, K. Kaneko, *J. Mater. Chem. A* **2019**, *7*, 19996.
- [231] Z. Gao, K. Jiang, Z. Lou, W. Han, G. Shen, *J. Mater. Chem. C* **2019**, *7*, 9648.
- [232] X. Su, H. Li, X. Lai, Z. Chen, X. Zeng, *ACS Appl. Mater. Interfaces* **2018**, *10*, 10587.
- [233] S. Zhang, L. Wen, H. Wang, K. Zhu, M. Zhang, *J. Mater. Chem. C* **2018**, *6*, 5132.
- [234] S. H. Jeong, S. Zhang, K. Hjort, J. Hilborn, Z. Wu, *Adv. Mater.* **2016**, *28*, 5830.
- [235] A. Mahdavi, L. Ferreira, C. Sundback, J. W. Nichol, E. P. Chan, D. J. D. Carter, C. J. Bettinger, S. Patanavanich, L. Chignozha, E. Ben-Joseph, A. Galakatos, H. Pryor, I. Pomerantseva, P. T. Masiakos, W. Faquin, A. Zumbuehl, S. Hong, J. Borenstein, J. Vacanti, R. Langer, J. M. Karp, *Proc. Natl. Acad. Sci. U. S. A.* **2008**, *105*, 2307.
- [236] W. G. Bae, D. Kim, M. K. Kwak, L. Ha, S. M. Kang, K. Y. Suh, *Adv. Healthc. Mater.* **2013**, *2*, 109.
- [237] V. Barreau, R. Hensel, N. K. Guimard, A. Ghatak, R. M. McMeeking, E. Arzt, *Adv. Funct. Mater.* **2016**, *26*, 4687.
- [238] S. Y. Yang, E. D. O’Cearbhaill, G. C. Sisk, K. M. Park, W. K. Cho, M. Villiger, B. E. Bouma, B. Pomahac, J. M. Karp, *Nat. Commun.* **2013**, *4*, 1.
- [239] K. Y. Seong, M. S. Seo, D. Y. Hwang, E. D. O’Cearbhaill, S. Sreenan, J. M. Karp, S. Y. Yang, *J. Control. Release* **2017**, *265*, 48.

- [240] R. C. Webb, A. P. Bonifas, A. Behnaz, Y. Zhang, K. J. Yu, H. Cheng, M. Shi, Z. Bian, Z. Liu, Y. S. Kim, W. H. Yeo, J. S. Park, J. Song, Y. Li, Y. Huang, A. M. Gorbach, J. A. Rogers, *Nat. Mater.* **2013**, *12*, 938.
- [241] D. Son, J. Lee, S. Qiao, R. Ghaffari, J. Kim, J. E. Lee, C. Song, S. J. Kim, D. J. Lee, S. W. Jun, S. Yang, M. Park, J. Shin, K. Do, M. Lee, K. Kang, C. S. Hwang, N. Lu, T. Hyeon, D. H. Kim, *Nat. Nanotechnol.* **2014**, *9*, 397.
- [242] M. Amjadi, S. Sheykhansari, B. J. Nelson, M. Sitti, *Adv. Mater.* **2018**, *30*, 1704530.
- [243] Z. Li, M. Zhu, J. Shen, Q. Qiu, J. Yu, B. Ding, *Adv. Funct. Mater.* **2020**, *30*, 1908411.
- [244] A. Miyamoto, S. Lee, N. F. Cooray, S. Lee, M. Mori, N. Matsuhisa, H. Jin, L. Yoda, T. Yokota, A. Itoh, M. Sekino, H. Kawasaki, T. Ebihara, M. Amagai, T. Someya, *Nat. Nanotechnol.* **2017**, *12*, 907.
- [245] H. Araki, J. Kim, S. Zhang, A. Banks, K. E. Crawford, X. Sheng, P. Gutruf, Y. Shi, R. M. Pielak, J. A. Rogers, *Adv. Funct. Mater.* **2017**, *27*, 1604465.
- [246] L. Y. Chen, B. C. K. Tee, A. L. Chortos, G. Schwartz, V. Tse, D. J. Lipomi, H. S. P. Wong, M. V. McConnell, Z. Bao, *Nat. Commun.* **2014**, *5*, 1.
- [247] L. Teng, K. Pan, M. P. Nemitz, R. Song, Z. Hu, A. A. Stokes, *Soft Robot.* **2019**, *6*, 82.
- [248] S. Li, J. Wang, W. Peng, L. Lin, Y. Zi, S. Wang, G. Zhang, Z. L. Wang, *Adv. Energy Mater.* **2017**, *7*, 1602832.
- [249] S. Gong, W. Cheng, *Adv. Energy Mater.* **2017**, *7*, 1700648.
- [250] X. Hu, Z. Huang, X. Zhou, P. Li, Y. Wang, Z. Huang, M. Su, W. Ren, F. Li, M. Li, Y. Chen, Y. Song, *Adv. Mater.* **2017**, *29*, 1703236.
- [251] R. Kumar, J. Shin, L. Yin, J.-M. You, Y. S. Meng, J. Wang, *Adv. Energy Mater.* **2017**, *7*, 1602096.
- [252] S. Xu, Y. Zhang, L. Jia, K. E. Mathewson, K. I. Jang, J. Kim, H. Fu, X. Huang, P. Chava, R. Wang, S. Bhole, L. Wang, Y. J. Na, Y. Guan, M. Flavin, Z. Han, Y. Huang, J. A. Rogers, *Science*. **2014**, *344*, 70.
- [253] Y. Khan, M. Garg, Q. Gui, M. Schadt, A. Gaikwad, D. Han, N. A. D. Yamamoto, P. Hart, R. Welte, W. Wilson, S. Czarnecki, M. Poliks, Z. Jin, K. Ghose, F. Egitto, J. Turner, A. C. Arias, *Adv. Funct. Mater.* **2016**, *26*, 8764.
- [254] M. K. Choi, J. Yang, K. Kang, D. C. Kim, C. Choi, C. Park, S. J. Kim, S. I. Chae, T. H. Kim, J. H. Kim, T. Hyeon, D. H. Kim, *Nat. Commun.* **2015**, *6*, 1.
- [255] W. Kim, S. Kwon, Y. C. Han, E. Kim, K. C. Choi, S.-H. Kang, B.-C. Park, *Adv. Electron. Mater.* **2016**, *2*, 1600220.
- [256] C.-C. Hung, Y.-C. Chiu, H.-C. Wu, C. Lu, C. Bouilhac, I. Otsuka, S. Halila, R. Borsali, S.-H. Tung, W.-C. Chen, *Adv. Funct. Mater.* **2017**, *27*, 1606161.
- [257] J. Kim, D. Son, M. Lee, C. Song, J. K. Song, J. H. Koo, D. J. Lee, H. J. Shim, J. H. Kim, M. Lee, T. Hyeon, D. H. Kim, *Sci. Adv.* **2016**, *2*, e1501101.
- [258] A. Polywka, T. Jakob, L. Stegers, T. Riedl, P. Görrn, *Adv. Mater.* **2015**, *27*, 3755.
- [259] Y.-Y. Lee, H.-Y. Kang, S. H. Gwon, G. M. Choi, S.-M. Lim, J.-Y. Sun, Y.-C. Joo, *Adv. Mater.* **2016**, *28*, 1636.
- [260] J. Kim, R. Ghaffari, D. H. Kim, *Nat. Biomed. Eng.* **2017**, *1*, 1.
- [261] W. Gao, S. Emaminejad, H. Y. Y. Nyein, S. Challa, K. Chen, A. Peck, H. M. Fahad, H. Ota, H. Shiraki, D. Kiriya, D. H. Lien, G. A. Brooks, R. W. Davis, A. Javey, *Nature* **2016**, *529*, 509.
- [262] H. Lee, T. K. Choi, Y. B. Lee, H. R. Cho, R. Ghaffari, L. Wang, H. J. Choi, T. D. Chung, N. Lu, T. Hyeon, S. H. Choi, D. H. Kim, *Nat. Nanotechnol.* **2016**, *11*, 566.
- [263] Y. Khan, A. Thielens, S. Muin, J. Ting, C. Baumbauer, A. C. Arias, *Adv. Mater.* **2019**, 1905279.
- [264] L. Teng, K. Jeronimo, T. Wei, M. P. Nemitz, G. Lyu, A. A. Stokes, *J. Micromech. Microeng.* **2018**, *28*, 054001.